Master Thesis

Phase-field Modeling of Crystal Growth during Deformation

Tan Xu

Department of Ferrous Technology

(Computational Metallurgy)

Graduate Institute of Ferrous Technology

Pohang University of Science and Technology

2010

Phase-field Modeling of Crystal Growth during Deformation

Phase-field Modeling of Crystal Growth during Deformation

by
Tan Xu
Department of Ferrous Technology
(Computational Metallurgy)
Graduate Institute of Ferrous Technology
Pohang University of Science and Technology

A thesis submitted to the faculty of Pohang University of Science and Technology in partial fulfillments of the requirements for the degree of Master of Science in the Graduate Institute of Ferrous Technology

Pohang, Korea
21. June. 2010
Approved by
Prof. Rongshan, Qin _____
Prof. Bhadeshia. H.K.D.H_____
Major Advisor

Phase-filed Modeling of Crystal Growth during Deformation

Tan Xu

This dissertation is submitted for the degree of Master of Science at the Graduate Institute of Ferrous Technology of Pohang University of Science and Technology. The research reported herein was approved by the committee of Thesis Appraisal

21. June. 2010

Thesis Review Committee
Chairman: Barlat, Frederic _____
Member: Kim, In Gee _____
Member: Suh, Dong-Woo _____

MFT

20081013 Tan Xu

Phase-field Modeling of Crystal Growth during Deformation

Department of Ferrous Technology (Computational Metallurgy) 2010

Advisor: Professor Rongshan, Qin and Professor H.K.D.H.Bhadeshia

Text in English

ABSTRACT

A method to compute crystal growth during materi als deformation has been developed. This is done b y firstly extension of the numerical solution of the recent developed phase-field model from regular l attice to the irregular lattice. Accurate mathematic s and discrete algorithms are derived for solving p hase-field governing equation in generic spatial co nfigurations. The homogeneous deformation is mod eled as vector operator on each lattice. The metho d enables the simulation of warm rolling, a thermo mechanical processing method possessing huge po

tential for making high quality steels but far behind the scientific understanding due to the complex nature of that the phase transition and deformation take place simultaneously. Numerical simulation of three-dimensional crystal growth in deformation demonstrates interesting morphological evolution, and is understood by combining crystal anisotropy and free energy minimization.

Contents

Abstract----------V
Contents----------VI-VII
Nomenclature----------VIII-IX

I. **Introduction**
1.1 **Overview**---------- 1-3

1.2 **Phase-field model**---------- 4-14
1.2.1Overview---------- 4
1.2.2Interface---------- 4-5
1.2.3 Governing equation---------- 5-8
1.2.4 Interfacial anisotropy---------- 9-11
1.2.5 Parameters specification---------- 11-14

1.3 Homogeneous deformation---------- 14-24
1.3.3 Types of homogeneous deformation---------- 14-16
1.3.4 Effects of homogeneous deformation---------- 16-21
1.3.5 Simple shear deformation---------- 21
1.3.6 Governing equation---------- 22-24

1.4 **Aim of the work**---------- 24-25

II. Numerical methodology
2.1 **Overview**---------- 26-27

2.2 **Numerical procedure**---------- 27-31
2.2.1 Lattice properties---------- 27
2.2.2 Nucleation---------- 28
2.2.3 Time step---------- 28-29
2.2.4 Non-dimensionalization---------- 29-30
2.2.5 Discretization---------- 30-31

2.3 Finite-difference method

2.3.1 Overview---------- 31-32

2.3.2 General finite-difference method---------- 32-34

2.3.3 Application---------- 35-40

2.4 Coordinate transformation

2.4.1 General coordinate transformation---------- 41-44

2.4.2 Application---------- 44-45

2.5 **Conclusion**---------- 45-46

III. Simulation and discussion

3.1 **Overview**---------- 47

3.2 Simulation---------- 47-58

3.2.1 System diagram---------- 47-49

3.2.2 Parameters of simulation---------- 49-51

3.2.3 Results---------- 52-58

3.3 **Discussion**---------- 59-67

3.4 **Conclusion**---------- 68-69

IV. **Conclusion**---------- 60-71

Reference ---------- 72-74

Appendix A---------- 75-81

Acknowledgements---------- 82

Nomenclature

ϕ	Phase-field parameter
T	Temperature
c	Composition
ε	Gradient energy coefficient
$\overline{\varepsilon}$	Mean value of gradient energy coefficient
G	Free energy
g_0	Free energy per unit volume of a homogeneous phase of composition c at temperature T
g_b	Chemical free energy of bulk phase
ω	Coefficient reflecting the excess free energy
$\hat{n}$	Normal direction to the interface
$k_i (i = 1, 2, 3)$	Coefficients reflecting anisotropy

M_ϕ	Phase-field mobility
t	time
2λ	Interface thickness
σ	Interface energy
v	Interface propagation rate
Δx	Lattice distance
γ	Radius of spherical seed
L	Characteristic length
D_c	Carbon diffusivity in steel
R	Gas constant
V_m	Molar volume of the material
u^h	Grid function
Ω	Grid cell
l	Contour of the cell
T_c	Martensitic transition temperature

Chapter 1

Introduction

1.1 Overview

Rolling services the purposes of breaking down materials dimension as well as improving their mechanical properties. Figure 1.1 illustrates schematically one of the simplest rolling processes. There are many different kinds of rolling in terms of the strain and stress relationships. Sometimes those different types of rolling can be combined together to achieve designed geometry or properties. Even in the simple case as illustrated in Fig. 1.1 where there is only one type of deformation, several passes may be made to achieve the desired decrease in thickness.

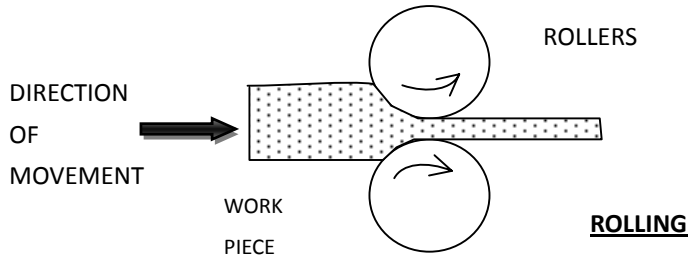

Figure 1.1: schematics of rolling process.

Rolling can be categorized into hot, cold and warm works. The former two deformations take place in single-phase area, i.e. no considerable phase transition is going on during materials deformation. Most of the engineering applications in the current stage are felled into those two categories and are called hot rolling and cold rolling, separately.

The present work focuses on the third category - warm rolling. The rolling temperature is at the austenite-ferrite two-phase region in Fe-C phase diagram instead of just one phase existence, and the fraction of each phase can change via phase transition [1]. In comparing with hot rolling, warm working can make material closer to its final shape and with better mechanical properties. In comparison with cold rolling, it saves energy and avoids some heat treatments such as baken hardening and annealing and removing residual stress. It is also found the warm rolling in the upper ferritic region produce profitable microstructure. The comprehensive microstructure evolution in warm rolling provides an economical and technically viable operation.

Whilst the metallurgy of the hot and cold rolling of steel has been extensively studied, that of warm rolling has not received anywhere near the same amount of attention. This is probably because there has been much less industrial interest in this process. However, in

recent years there is an increasing need to understand the metallurgy of warm rolling, which particular attention being paid to factors influencing the properties of the final product. A number of investigations have been done to consider the micro and macro behavior of material during warm rolling and phase transition [2-3]. The effect of rolling speed on strain aging phenomena in warm rolling of the carbon steel has been investigated [4]. The deformation microstructure of various warm rolled steels was characterized and its influence upon the subsequent annealing behavior was conducted [5-6]. However, warm rolling is still far from a common process in the context of the huge quantities of steel manufactured in the world, because the full mechanisms involved in warm rolling process to generate the final microstructure and crystallographic structures are not understood. Thus, understanding of material behavior is of importance for designing a proper rolling process and more studies are required to understand the phenomenon of this process.

During warm rolling process, homogeneous deformation occurs in phase transition affecting grain geometry. It brings out not only the direct distortion of grain morphology in a manner to comply with strain, but also changes the area of grain size and length of the grain edges. As a consequence, it affects the final microstructure and properties of the product through in the two-phase transition region.

It is essential for controlling the mechanical properties of steels to predict the transformation kinetics and the morphology of microstructure by using the numerical simulation. In previous work, some mathematical models integrated with numerical technique were used to predict material behavior during warm rolling. The numerical model provides a systematic way of predicting the mechanical properties of steel depending on the microstructure.

The mechanical properties of steels, such as strength, toughness and ductility are characterized not only by the composition and volume fraction of the constituent phase, but also the microscopic configuration of the microstructure that is produced during thermomechanical process. Therefore, it is necessary, to for the development of new steels, to construct a numerical model that will enable the systematic investigation between the microstructure and mechanical properties of steels with a high accuracy. Recently, as powerful tools predicting for the microstructure evolution during solidification, phase transformation and recrystallization in the micro- and mesoscale regions, the time-dependent Ginzburg-Landau theory and phase-field method has been widely applied [7]. In order to predict the mechanical properties of steels and develop the new desired steels, it is essential to conduct a coupled numerical simulation using the phase-field model. Here a coupled simulation by the phase-field method combined with the finite-difference

method on the generic grids is developed to model the microstructure formation for steel, which are undergoing deformation during the phase transition.

1.2 Phase-field model

1.2.1 Overview

Phase-field models are widely used for the simulation of grain growth in various phase transformations. It is used as a theory and computational tool for the prediction of the growth of modeled morphologies and complicated microstructure in materials. It was first introduced by Fix [8] and Langer [9] and now has been applied successfully in solidification and other metallurgical problems.

In the model, the phase-field order parameter ϕ is introduced to represent the phase, taking on constant values indicative of each of the bulk phase and making a transition between values over the transition layer corresponds to the interface region which is a finite

width. For example, $\phi = 1$, $\phi = 0$ and $0 < \phi < 1$ represent the precipitate, matrix and interface respectively.

1.2.2 Interface

Phase field model is based on a diffuse-interface description. The interfaces between domains are identified by a continuous variation of the properties in a narrow region (Fig. 1a). In conventional modeling techniques for phase transformations and microstructure evolution, the interfaces between different domains are considered to be infinitely sharp (Fig. 1b), and a multi-domain structure is described by the position of the interfacial boundaries [7].

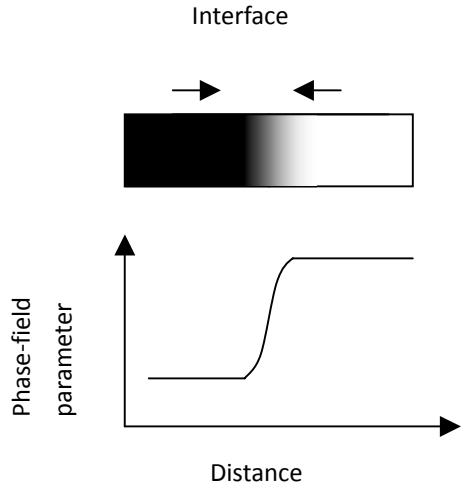

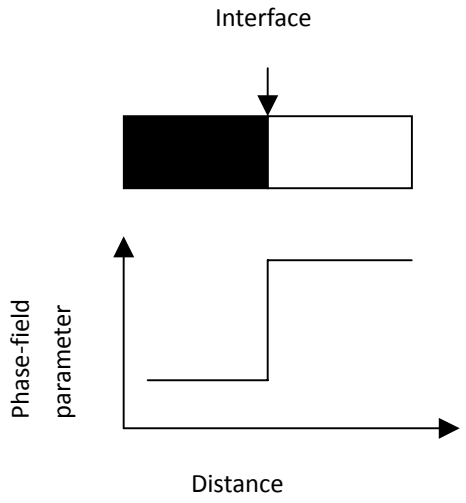

Figure 1.1: (a) Diffuse interface; (b) Sharp interface.

1.2.3 Governing equation

The total free energy G of the volume is then described in terms of the phase-field parameter ϕ and its gradients, and the rate at which the structure evolves with time is set in context of irreversible thermodynamics, and depends on how G varies with ϕ. Cahn and

Hilliard got the expression of g as free energy per unit volume of a heterogeneous system by considering a multivariate Taylor expansion [10-11]. Writing $g_0\{\phi, c, T\}$ as the free energy per unit volume of a homogeneous phase of composition c at temperature T, the expansion of g is [30]:

$$
\begin{aligned}
g = g_0 &+ \frac{\partial g_0}{\partial \nabla\phi}\nabla\phi + \frac{1}{2}\frac{\partial^2 g_0}{\partial(\nabla\phi)^2}\partial(\nabla\phi)^2 + \cdots + \frac{\partial g_0}{\partial \nabla^2\phi}\partial\nabla^2\phi + \frac{1}{2}\frac{\partial^2 g_0}{\partial(\nabla^2\phi)^2}(\nabla^2\phi)^2 + \cdots \\
&+ \frac{\partial g_0}{\partial \nabla c}\nabla c + \frac{1}{2}\frac{\partial^2 g_0}{\partial(\nabla c)^2}\partial(\nabla c)^2 + \cdots + \frac{\partial g_0}{\partial \nabla^2 c}\partial\nabla^2 c + \frac{1}{2}\frac{\partial^2 g_0}{\partial(\nabla^2 c)^2}(\nabla^2 c)^2 + \cdots \\
&+ \frac{\partial g_0}{\partial \nabla T}\nabla T + \frac{1}{2}\frac{\partial^2 g_0}{\partial(\nabla T)^2}\partial(\nabla T)^2 + \cdots + \frac{\partial g_0}{\partial \nabla^2 T}\partial\nabla^2 T + \frac{1}{2}\frac{\partial^2 g_0}{\partial(\nabla^2 T)^2}(\nabla^2 T)^2 + \cdots \\
&+ \frac{1}{2}\left[\frac{\partial^2 g_0}{\partial\nabla\phi\partial\nabla c}\nabla\phi\nabla c + \frac{\partial^2 g_0}{\partial\nabla\phi\partial\nabla T}\nabla\phi\nabla T + \frac{\partial^2 g_0}{\partial\nabla c\partial\nabla T}\nabla c\nabla T + \cdots\right] + \cdots \quad (1.1)
\end{aligned}
$$

Using mathematical method and limiting the Taylor expansion to first and second order terms, g is given by integrating over the volume V:

$$G = \int_V \left[g_0\{\phi, c, T\} + \frac{\varepsilon^2}{2}(\nabla\phi)^2 \right] dV \qquad (1.2)$$

where $\varepsilon^2 = \partial^2 g_0 / \partial(\nabla\phi)^2 - 2\partial(\partial g_0 / \partial\nabla^2\phi)/\partial\phi$ is the gradient energy coefficient which will be discussed later. In actual

computations ε gives an accurate description of interface properties such as the energy per unit area and anisotropy of interfacial energy.

In austenite and ferrite two-phase region, consider a phase β where $\phi = 1$ growing in α where $\phi = 0$ and with $0 < \phi < 1$ defining the interface. Thus, assuming g_0 as double-well potential shape, which can cover the entire domain of phase-field parameter, the expression conducted in previous work is [12]:

$$g_0\{\phi, c, T\} = h\{\phi\}\, g_0^{\alpha}\left\{c^{\alpha}, T\right\} + \left[1 - h\{\phi\}\right] g_0^{\beta}\left\{c^{\beta}, T\right\} + \frac{1}{4\omega}\phi^2(1-\phi)^2 \quad (1.3)$$

where $h = \phi^3(6\phi^2 - 15\phi + 10)$ [13]; g_0^{α} and g_0^{β} are the free energy densities of respective phase; c_0^{α} and c_0^{β} are the solute contents of these phase. ω is a coefficient which can be adjusted to fit the desired interfacial energy but has to be positive to be consistent with a double-well potential as opposed to one with two peaks.

According to the second law of thermodynamics, the driving force for microstructure evolution is the possibility to reduce the free energy of the system. Thus, the governing equation for phase

transition is derived from thermodynamic function of state by means of irreversible law of thermodynamics. Free energy is used to derive the kinetic equation by requiring that total free energy decreases monotonically in time. It can be expressed by:

$$\frac{\delta G(\phi, c, T)}{\delta t} \leq 0 \qquad (1.4)$$

and an expansion of this equation gives:

$$\left(\frac{\delta G}{\delta \phi}\right)_{c,T}\left(\frac{\partial \phi}{\partial t}\right)_{c,T}+\left(\frac{\delta G}{\delta c}\right)_{\phi,T}\left(\frac{\partial c}{\partial t}\right)_{\phi,T}+\left(\frac{\delta G}{\delta T}\right)_{\phi,c}\left(\frac{\partial T}{\partial t}\right)_{\phi,c} \leq 0 \quad (1.5)$$

In this research, we assume constant composition and isothermal conditions so equation (1.5) reduces to following format:

$$\left(\frac{\delta G}{\delta \phi}\right)_{c,T}\left(\frac{\partial \phi}{\partial t}\right)_{c,T} \leq 0 \qquad (1.6)$$

According to the theory of irreversible thermodynamics that the 'flux' is proportional to the 'force' then

$$\underbrace{\left(\frac{\partial \phi}{\partial t}\right)_{c,T}}_{flux} = -M_{\phi}\underbrace{\left(\frac{\delta G}{\delta \phi}\right)_{c,T}}_{force} \qquad (1.7)$$

Combining equation (1.6) and (1.7)

$$-M_\phi \left[\left(\frac{\delta G}{\delta \phi} \right)_{c,T} \right]^2 \le 0 \qquad (1.8) \text{ where } \; M_\phi \ge 0 .$$

Taking all the factors above, we can get

$$\frac{\delta G}{\delta \phi} = \frac{\partial g}{\partial \phi} - \varepsilon_\phi^2 \nabla^2 \phi \qquad (1.9)$$

So that

$$\frac{\partial \phi}{\partial t} = M_\phi \left[\varepsilon_\phi^2 \nabla^2 \phi - \frac{\partial g\{\phi\}}{\partial \phi} \right] \qquad (1.10)$$

Inserting equations (1.2) and (1.3) into (1.10) leads to

$$\frac{\partial \phi}{\partial t} = M_\phi \{ \frac{\partial}{\partial x} \left[|\nabla \phi|^2 \, \varepsilon(\hat{n}) \frac{\partial \varepsilon(\hat{n})}{\partial(\partial x)} \right] + \frac{\partial}{\partial y} \left[|\nabla \phi|^2 \, \varepsilon(\hat{n}) \frac{\partial \varepsilon(\hat{n})}{\partial(\partial y)} \right]$$

$$+ \frac{\partial}{\partial z} \left[|\nabla \phi|^2 \, \varepsilon(\hat{n}) \frac{\partial \varepsilon(\hat{n})}{\partial(\partial z)} \right] + \nabla \left[\varepsilon(\hat{n})^2 \nabla \phi \right] + \frac{1}{2\omega} \phi(1-\phi)(1-2\phi) - \frac{\partial g_0}{\partial \phi} \}$$

(1.11)

1.2.4 Interfacial anisotropy

Classical grain growth theories assume isotropic interface energies

and that all interfaces move by the same mechanism. However, it has been recognized for many decades that the mechanisms by which interfaces move depend to some extent on the interface anisotropy.

The so-called interface anisotropy came into the phase-field model by assuming that ϕ is orientation-dependent which relative to the crystal lattice [14].

Many theories have been developed to describe the interface anisotropy [15]. In this three dimensional simulation, a generic expression for interface anisotropy energy of crystals with cubic symmetry can be represented in simple format as [16]:

$$\varepsilon(\hat{n}) = \bar{\varepsilon}[k_0 + k_1(n_x^2 n_y^2 + n_y^2 n_z^2 + n_z^2 n_x^2) + k_2 n_x^2 n_y^2 n_z^2 + k_3(n_x^2 n_y^2 + n_y^2 n_z^2 + n_z^2 n_x^2)^2] \quad (1.12)$$

$$\hat{n} \equiv \frac{\vec{\nabla}\phi}{\left|\vec{\nabla}\phi\right|} \quad (1.13)$$

where $\hat{n}$ is the normal direction to the interface. $\bar{\varepsilon}$ is the mean value of gradient energy coefficient. k_0, k_1, k_2 and k_3 are coefficients.

Using Miller indices, it gives:

$$n_x = \frac{h}{\sqrt{h^2 + k^2 + l^2}} \quad (1.14)$$

$$n_y = \frac{k}{\sqrt{h^2 + k^2 + l^2}} \quad (1.15)$$

$$n_z = \frac{l}{\sqrt{h^2 + k^2 + l^2}} \quad (1.16)$$

where the normal vector to plane with Miller indices (hkl) plane is the direction $[hkl]$. The unit normal vector $\hat{n}$ has its Cartesian coordinates n_x, n_y and n_z. So equation (1.12) can be represented as:

$$\varepsilon(\hat{n}) = \bar{\varepsilon}[1 + k_1(\frac{h^2k^2 + k^2l^2 + l^2h^2}{(h^2 + k^2 + l^2)^2}) + k_2 \frac{h^2k^2l^2}{(h^2 + k^2 + l^2)^3} + k_3 \frac{(h^2k^2 + k^2l^2 + l^2h^2)^2}{(h^2 + k^2 + l^2)^4}] \quad (1.17)$$

k_1, k_2 and k_3 proved by experimental measurement of anisotropy surface energy or from microscopic numerical calculation such as embedded atom method [16]. For example, there are three sets of parameters as listed in Table 1.1.

	Case A	Case B	Case C
k_1	-0.863	0.395	0.0
k_2	0.402	0.00144	0.0
k_3	1.8655	0.2555	0.0

Table 1.1: Different sets of anisotropic coefficients

Using phase-field model, with these three sets of anisotropic coefficients grain morphology were demonstrated in Fig. 1.2.

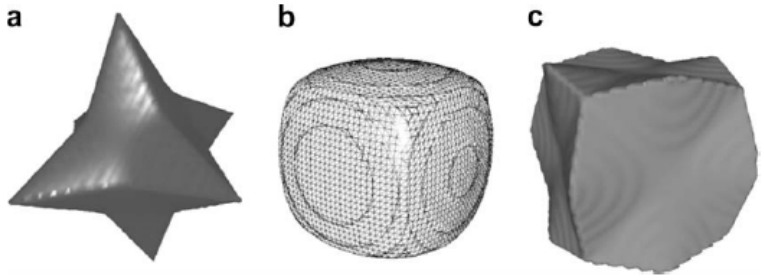

Fig. 1.2: Grain morphology at 5000 time steps under different interface anisotropy: (a) Case A, (b) Case B and (c) Case C. [16]

1.2.5 Parameter specification

In order to simulate the phase field governing equation, first thing should specify the parameters in the equation like mobility M, gradient energy coefficient ε and the interfacial fitting parameter ω. The general method for determination of phase-field model parameter is to manipulate the phase transition to the simplest case so that the unknown parameters show their macroscopic meaning.

Since in equilibrium state $\partial\phi/\partial t = 0$, equation (1.10) in one-dimensional system where the interface is constant is reduced to:

$$\varepsilon^2 \frac{d^2\phi}{dx^2} - \frac{1}{2\omega}\phi(1-\phi)(1-2\phi) = 0 \qquad (1.18)$$

The boundary condition:

$$\begin{cases} \phi = 1 & x = -\infty \\ \phi = 0 & x = +\infty \end{cases} \qquad (1.19)$$

The solution of equation (1.18) is:

$$\phi(x) = \frac{1}{2}\left[1 - \tan\frac{x}{2\sqrt{2\omega\varepsilon}}\right] \qquad (1.20)$$

Then we assume that

$$\lambda = 2\sqrt{2\omega\varepsilon} \qquad (1.21)$$

This gives a good approximation of interface thickness because form equation (1.20) we can get $\phi(\lambda) = 0.90025$ and $\phi(-\lambda) = 0.0975$. λ is called the half-interface thickness because the interface starts

from λ and ends at $-\lambda$.

Multiplying equation (1.18) with $d\phi / dx$ and integrating leads to

$$\frac{1}{2}\varepsilon^2\left(\frac{d\phi}{dx}\right)^2 = \frac{1}{4\omega}\phi^2(1-\phi)^2 \qquad (1.22)$$

The interface energy is all the excess energy at the interfacial region, which is

$$\sigma = \int_{-\infty}^{+\infty}\left[\frac{1}{2}\varepsilon^2\left(\frac{d\phi}{dx}\right)^2 + \frac{1}{4\omega}\phi^2(1-\phi)^2\right] = \varepsilon^2\int_{-\infty}^{+\infty}\left(\frac{d\phi}{dx}\right)^2 dx \qquad (1.23)$$

Using equation (1.20) and equation (1.23) leads to:

$$\sigma = \frac{\sqrt{2}\varepsilon}{12\sqrt{\omega}} \qquad (1.24)$$

Equations (1.21) and (1.24) give:

$$\sigma = \frac{1.1}{3\lambda}\varepsilon^2 \qquad (1.25)$$

Suppose the gradient energy coefficient has the following format:

$$\varepsilon(\hat{n}) = \varepsilon_0 + \varepsilon_1(n_x^2n_y^2 + n_y^2n_z^2 + n_z^2n_x^2) + \varepsilon_2 n_x^2n_y^2n_z^2 + \varepsilon_3(n_x^2n_y^2 + n_y^2n_z^2 + n_z^2n_x^2)^2$$

(1.26)

Bringing equation (1.26) into equation (1.25) and comparing the results with equation (1.12), it gives

$$\varepsilon_0 = \overline{\varepsilon} \qquad (1.27)$$

$$\varepsilon_1 = \frac{\lambda_0 k_1}{2\sqrt{k_0}} \qquad (1.28)$$

$$\varepsilon_2 = \frac{\lambda_0 k_2}{2\sqrt{k_0}} \qquad (1.29)$$

$$\varepsilon_3 = \frac{\lambda_0 k_3}{2\sqrt{k_0}} - \frac{\lambda_0 k_1^{\,2}}{8k_0\sqrt{k_0}} \qquad (1.30)$$

where $\lambda_0 = \sqrt{3\lambda / 1.1}$. These equations fully determine the coefficients of gradient energy coefficient function in terms of the coefficients in the anisotropic interface energy function.

So the parameters ε , ω and M_ϕ in the phase-field governing equations need to be matched with the interface energy σ , interface thickness 2λ and interface propagation rate v [17-18].

The width of the interface, 2λ , is treated as a parameter which is adjusted to minimize computational expense or using some other criterion such as the resolution of detail in the interface; values of the

interfacial energy per unit area, σ , may be available from experimental measurements. The mobility M_ϕ is determined experimentally.

Actually, the use of the phase-field model as an accurate computation tool for the computation of two or three-dimensional solid shapes will require more sophisticated numerical algorithms, possibly employing adaptive finite difference techniques.

1.3 Homogeneous deformation

1.3.1 Types of homogeneous deformation

The rolling process can be modelled as a continuous process of deformation for long parts of constant cross section, in which a reduction of the cross-sectional area is achieved by compression between two or more rotation rolls.

Deformation in the rolling process leads to a change in the shape of material due to an applied stress such as tensile, compressive, shear, torsion, and etc. Figure 3 shows these four principal ways in which a

load may be applied.

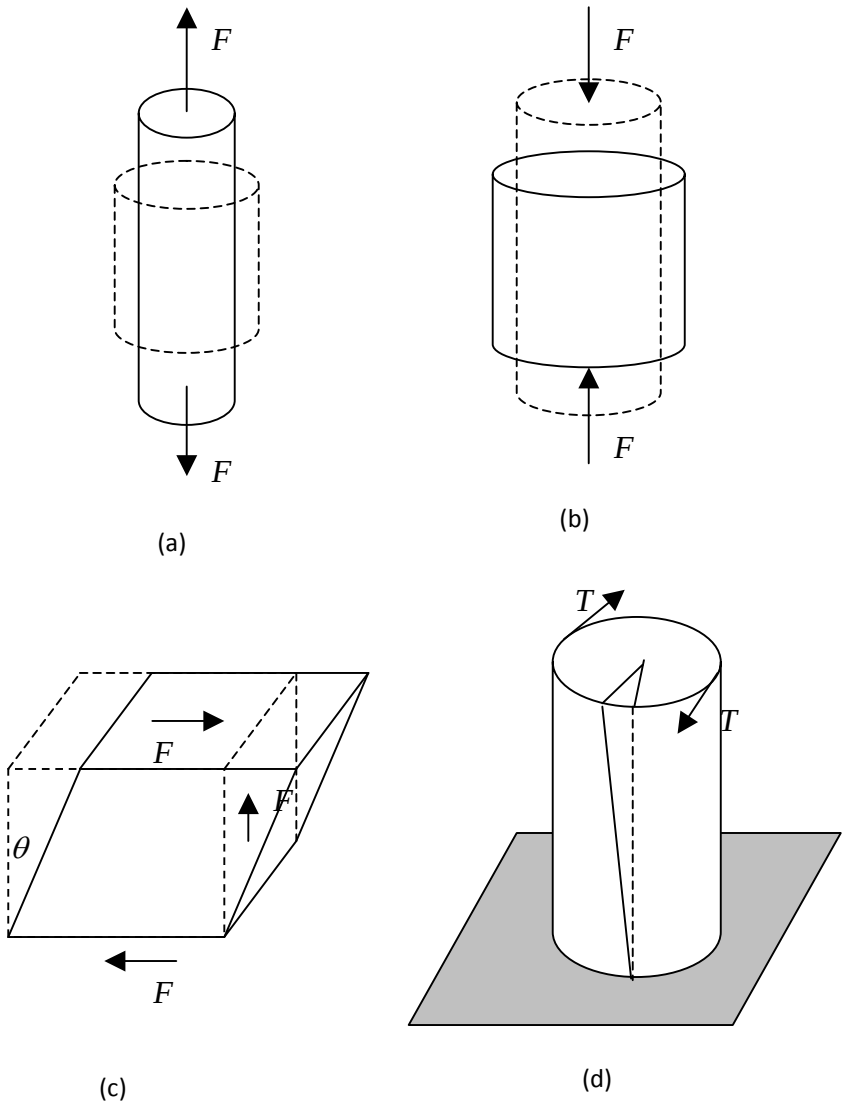

Figure 1.4: (a) Schematic illustration of how a tensile load produces an elongation and positive linear strain. Dashed lines represent the shape before deformation; solid lines, after deformation. (b) Schematic illustration of how a compressive load produces

contraction and a negative linear strain. (c) Schematic representation of shear strain γ, where $\gamma = \tan\theta$. (d) Schematic representation of torsional deformation (i.e., angle of twist ϕ) produced by an applied torque T.

As showed in Figure 4, tension is the magnitude of the pulling force exerted by a string, cable, chain or similar object on another object. Compress deformation is the result of the subjection of a material to compressive stress, resulting in reduction of volume. Shear deformation is continuum mechanics refers to a mechanical process that causes a deformation of a material substance in which parallel internal surfaces slide past one another. It is induced by a shear stress in the material. Torsion is the twisting of an object due to an applied torque.

1.3.2 Effects of homogeneous deformation

In previous work [19], the effect of four principal deformations on the grain boundary surface area per unit volume and edge length per unit volume is examined. Figs. 1.5, 1.6 and 1.7 show the results of different types of deformation.

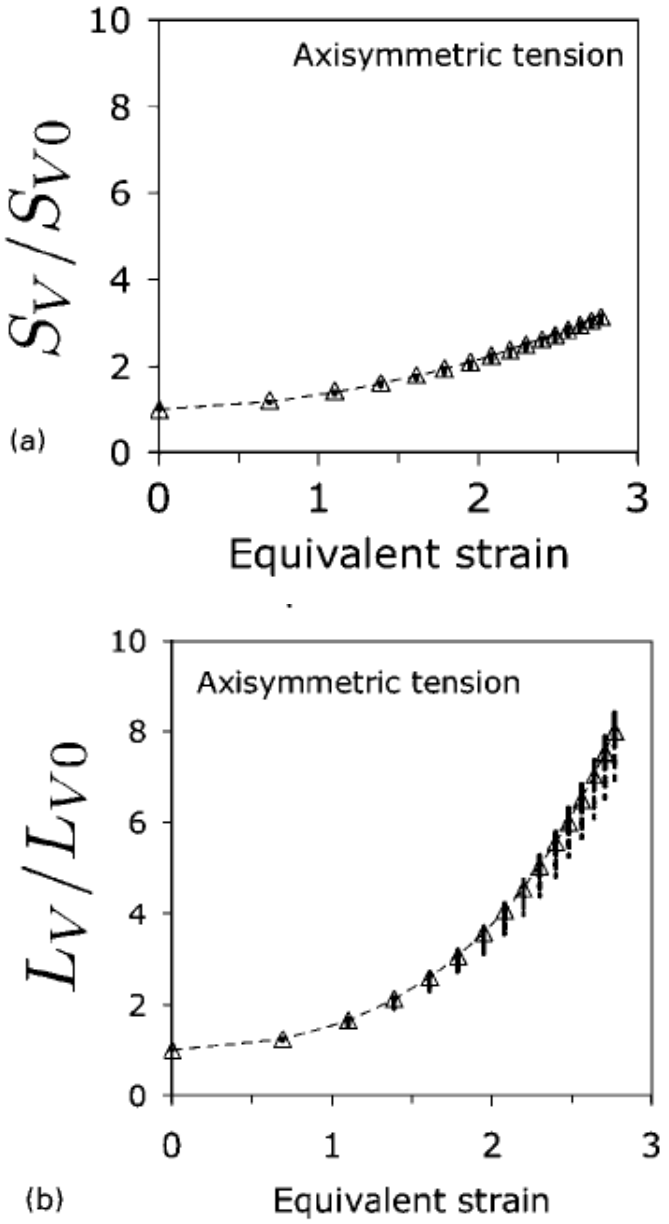

Figure 1.5: Calculation for axisymmetric tension. (a) Area ratio versus equivalent strain. (b) Edge ratio versus equivalent strain. [19]

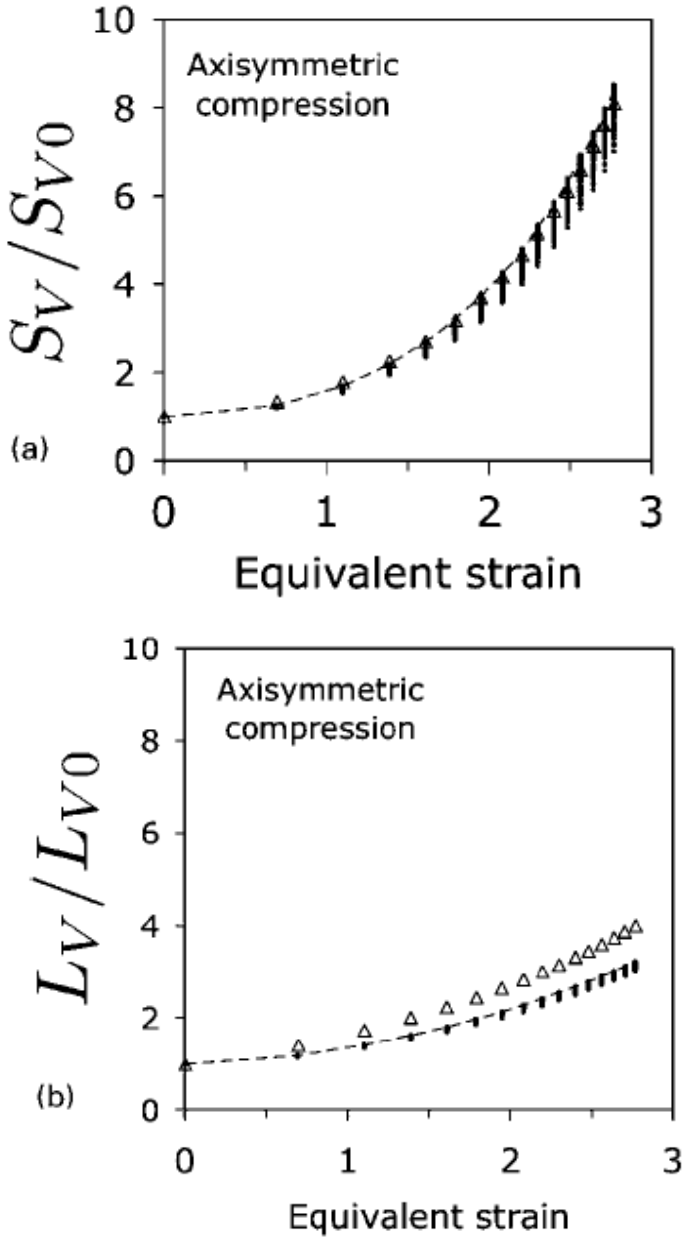

Figure 1.6: Calculation for axisymmetric compression. (a) Area ratio versus equivalent strain. (b) Edge ratio versus equivalent strain. [19]

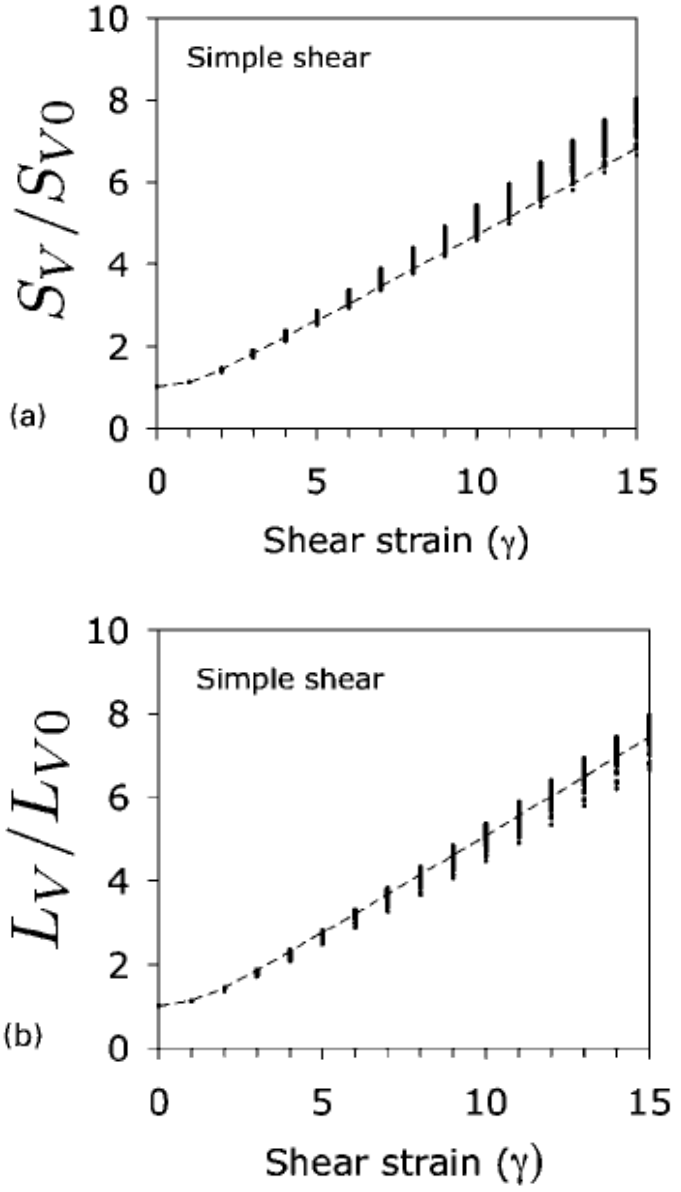

Figure 1.7: Calculation for simple shear. (a) Area ratio versus equivalent strain. (b) Edge ratio versus equivalent strain [19].

Depending on the type of material, size and geometry of the object, and the forces applied, various types of deformation may result, like elastic deformation and plastic deformation. Elastic deformation is reversible. Once the forces are no longer applied, the object returns to its original shape. Plastic deformation describes the deformation of a material undergoing non-reversible changes of shape in response to applied forces. It mainly causes two kinds of microstructure evolution. One is change of dislocation density which related to driving force for nucleation and growth of recrystallised grains formed either dynamically or statically. Another one is the direct grain distortion which causes the change of grain interface orientation showed in Figure. 1.8. Furthermore, it will change the subsequent interface migration pattern and eventually lead to the change of grain morphology.

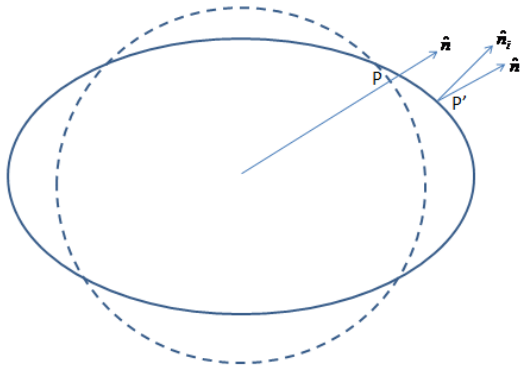

Figure 1.8: Schematic diagram shows the interface orientation evolution during deformation. The point P and $\hat{n}$ are the position and its orientation at the origination grain. P' and $\hat{n}_i$ are those at deformed grain.

According to the phase-field model, it is well known that the interface anisotropy plays important role in grain microstructure evolution. The anisotropy has been considered since the early stage development of phase-field models. In equation (1.13), $\hat{n}$ is the normal direction to the interface which is strongly related to the grain morphology.

1.3.3 Simple shear deformation

When a force of any magnitude is applied to a solid body the body becomes distorted; that is, some part of the body moves with respect

to some neighboring portion as showed in Figure 1.9. As a result of this displacement the atomic attractive forces in the body set up restoring forces that resist the alteration and tend to restore the body to its original shape. The restoring force in a deformed body is termed stress. The dimensional change produced by an applied force is called strain.

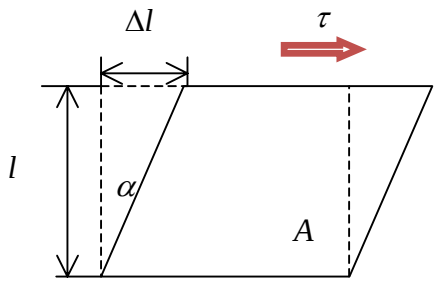

Figure 1.9: Two-dimensional geometric shear deformation of a finitesimal material element

The formula for the shear stress is:

$$\tau = \frac{F}{A} \qquad (1.31)$$

where τ is the shear stress, F is the force applied and A is the cross sectional area. The shear strain is defined as the change in angle α showed in Figure 1.9. In simple shear deformation, one direction remains constant and everything else rotates relative to it [20].

1.3.4 Governing equation

The grain morphology evolution under homogeneous deformation has been studied comprehensively [19, 21]. Once the grain structure is defined, it is possible to elastically deform it by applying an appropriate mathematical deformation matrix to each vertex.

For homogeneous deformation, a vector U is deformed into V following the rule of

$$\begin{pmatrix} S_{11} & S_{12} & S_{13} \\ S_{21} & S_{22} & S_{23} \\ S_{31} & S_{32} & S_{33} \end{pmatrix} \begin{pmatrix} U_1 \\ U_2 \\ U_3 \end{pmatrix} = \begin{pmatrix} V_1 \\ V_2 \\ V_3 \end{pmatrix} \qquad (1.32)$$

where S is the deformation matrix [11]. The elements of S take different values to represent various types of homogeneous deformation. Table 1.2 illustrates the non-zero element of S matrix for four kinds of simple homogeneous deformations.

Type	S_{11}	S_1	S_{13}	$S_{\cdot}$	S_{22}	S_{23}	S_{31}	S_{32}	S_{33}
Plane strain compression	≥ 1	0	0	0	1	0	0	0	$1/S_{11}$
Axisymmetric compression	$1/\sqrt{S_{33}}$	0	0	0	$1/\sqrt{S_{33}}$	0	0	0	≤ 1
Axisymmetric tension	≥ 1	0	0	0	$1/\sqrt{S_{11}}$	0	0	0	$1/\sqrt{S_{11}}$
Simple shear	1	0	+ve	0	1	0	0	0	1

Table 1.2: Volume preserving deformation. The convention used is that $S_{11} > S_{22} > S_{33}$

The grain shape evolution in homogeneous deformation can be calculated by application of equation (1.32) to every pixel of the grain body. For polyhedron grains, the morphological progressing is computable by just considering the conversion of grain vertexes during deformation [19]. Figure 1.10 demonstrated the changes of shape of two neighbored grains before and after simple deformation by vertexes transformation.

(a)

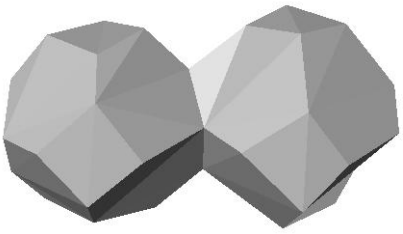

(b)

(c)

(d)

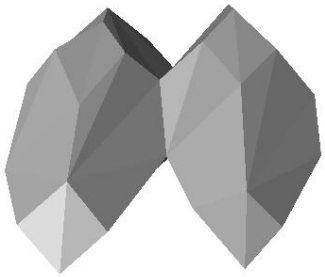

(e)

Figure 1.10: Grain shapes at (a) No-deformed grains; (b) Plain strain deformation; (c) Axisymmetric tension; (d) Axisymmetric compression; (e) Simple shear.

Furthermore, in terms of geometric concerns, equation (1.32) can be applied to transform the lattices using finite difference method to cope with the phase-field governing equation, which would change the grain interface orientation. This enables the integration of phase transition simulation with deformation simulation.

1.4 Aim of the work

The phase transformation during homogeneous deformation in steel is the fundamental important phenomenon for understanding warm rolling because the morphology of grain in steel plays important role on mechanical properties of the steel.

The microstructure changes during deformation process, with an increase in the grain geometry and grain distortion. The grain distortion induced by the elastic deformation also causes the change of grain interface orientation, which is relative to the $\varepsilon(\hat{n})$ value in phase-field model. This will result in completely different grain morphology and change the microstructure development during deformation while phase transition process in comparison of deformation after phase transition process.

In the previous studies, the formation and morphology of grain growth for phase transition from austenite has been simulated. However, to the author's knowledge, no phase-field model, which can treat the phase transformation under deformation, has been proposed. In order to predict the microstructure evolution during warm rolling, including the consequences on elementary mechanical properties, a new phase-field model, which is able to describe the phase transformation accompanying with the elastic deformation should be developed. Due to the complex inter-connection between deformation parameters and grain growth, more studies are still required in order to understand material behavior during warm rolling processes.

The main purpose of this study is to enable us to perform an integrated numerical simulation for the microstructure design of phase transition while rolling by coupling the phase-field model with homogeneous deformation method. Grain growth in phase transition is computed by phase-field model while the grain shape deformation is calculated by transforming grid coordinates according to homogeneous deformation matrix.

In the following section, we will reformulate the governing equation of the phase-field model to simulate the grain growth with

homogeneous deformation, including effects of grain geometry, and corresponding anisotropy parameters. We then provide detailed derivation of numerical methods. Finally, computed results for microstructure evolution of grain growth at different times and the effect of homogeneous deformation on the grain morphology are conducted concerning accuracy of the numerical method.

Chapter 2

Numerical methodology

2.1 Overview

In the past, the phase-field simulations showed that it is a general and powerful technique for simulating the evolution of relatively complex morphologies. Simulation could give important insights into the role of specific material or process parameters on the microstructure evolution in solidification and the shape and spatial distribution of precipitates in phase transformation process.

In the phase-field model, the temporal evolution of the phase-field variables, which represent the morphological evolution of the grains or domains in the system, is given by a set of coupled partial differential equations, one equation for each variable. In phase-field simulation, the results were rather qualitative and for real alloys the complicate quantitative simulation is difficult. The governing

equations in the model contain many phenomenological parameters and they are difficult to determine for real alloys. Moreover, massive computer resources are required to resolve the evolution of the phase-field variable at the interfaces appropriately and, at the same time, cover a system with realistic dimensions.

In this section, we give the steps in phase-field model and provide some of the numerical results with particular consideration when solving partial derivate equations of the second order factor for phase-field parameter $\phi(x,t)$ by the generalized finite difference method.

2.2 Numerical procedure

2.2.1 Lattices properties

Firstly, we initialize the lattices properties. We define suitable lattices to represent the space that occupied by material. At the initial condition, the lattice distance Δx is uniform and it must be fine enough to make sure there are a few grid points within the interfacial region to resolve the interfacial profile of the phase-field variables. Therefore, in this simulation the lattice distance is chosen as the one quarter of the interface thickness so that four lattices can cover the

interface. [22-23]

For the lattice depicted in Figure 2.1, the set of algebraic equation in the simulation contains $N_1 \times N_2 \times N_3$ equations and the same number of unknowns for each phase-field variable.

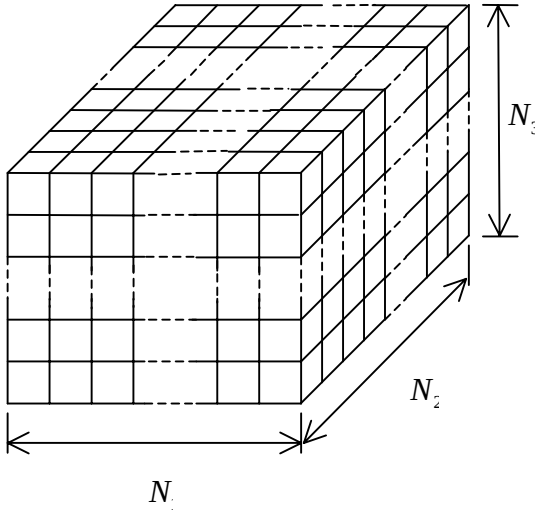

Figure 2.1 Lattices depiction at initial condition.

2.2.2 Nucleation

The formation of a crystal involves nucleation. Basically, if the nucleation occurs on a surface, such as a boundary of the system, or on other body, such as a dust particle, it is heterogeneous nucleation. If the structure and interatomic spacing of the surface on which nucleation takes place approximate those of the crystal, growth on

the surface can resemble growth on a normal seed. This is called epitaxial growth. If the nucleation occurs in the absence of a surface, that is, in the bulk of unit cell, it is homogeneous.

The model of this work focus on growth of single crystal, which occurs in the centre of the unit cell. Therefore, the second step is to put the nuclei manually to the lattice space according to the classical nucleation theory. The initial condition is to put a spherical seed with a radius of r at the centre of the logistic frame with phase-field order parameter configures to [16]

$$\begin{cases} \phi(r,t=0)=1 & for \quad r \le \Delta x \\ \phi(r,t=0)=\dfrac{2}{1+\exp(r-1)} & for \quad \Delta x < r < 4\Delta x \\ \phi(r,t=0)=0 & for \quad r \ge 4\Delta x \end{cases} \qquad (2.1)$$

Then all the lattices should be specified with the initial value of its phase-field order parameter ϕ, solute composition c and temperature T. In the processing, the lattice with $0.1<\phi<0.9$ is interface, $\phi<0.1$ is α and $\phi>0.9$ is β phase.

2.2.3 Time step

The third step is to define the proper time step, which affects the

stability of the finite-difference scheme which used for discreting the governing equation of phase-field model. At each time step, the value of the phase-field variables must be computed for all the grid points. In this simulation, for the stability of computation, we can directly use the necessary $\Delta t \le \frac{\Delta x^2}{2}$, where Δx is the length of the lattice. Moreover, smaller lattice spacing involves a smaller time step in order to maintain numerical stability. Because of this, large computer memory is also required to treat the huge algebraic systems of equations with many unknown.

2.2.4 Non-dimensionalization

The fourth step is to non-dimensionalize the governing equations for phase-field model. For the sake of computational stability, it is normal to use dimensional variables in the governing equations so that the occurrence of very small or very large numbers is avoided.

The parameters that used in equation (1.11) are non-dimensionalized by using [24]:

$\Delta\tilde{x} = x / L$, $\Delta\tilde{t} = 0.3\Delta\tilde{x}^2 / D_c$, $\tilde{M}_\phi = L^2 RT_c / D_c V_m$,

$\tilde{\varepsilon}_0 = \varepsilon_0 \sqrt{V_m / RT_c} / L$, $\tilde{\omega} = \omega RT_c / V_m$ and

$\tilde{g}_0 - \tilde{g}_1 = (g_1 - g_0)V_m / (RT_c)$. $L = 10\text{nm}$ is defined the characteristic length. $D_c = 10^{-6}\text{m}^3/\text{mol}$ is the carbon diffusivity in steel [27]. $R = 8.31\text{J}\cdot\text{K}^{-1}\text{mol}^{-1}$ is the gas constant. $V_m = 7.18\times10^{-6}\text{m}^3/\text{mol}$ is the molar volume of the material. $T_c = 369.8^{\circ}\text{C}$ is actually the martensitic transition temperature of Fe_0.4wt%C steel.

After non-dimensionalizing the variables, they range roughly between 0 and 1 and they are unnormailsed when interpreting the outputs of the model.

Furthermore, to make sure that all the parameters are chosen with practical ground rather than from pure fiction, the martenstic transition of Fe_0.4wt%C steel at 250°C is referenced, MTDATA thermodynamics database gives $g_0 = -1.73\times10^{9}\text{J/m}^2$ and $g_1 = -2.09\times10^{9}\text{J/m}^2$. $k_0 = 800\text{erg/cm}^2$ is the experimental value of interface energy in steel [26].

2.2.5 Discretization

The fifth step which is one of the most important steps is to discrete

the governing equation of phase-field model. In the present work finite difference formula is given for partial derivative equations of the first and second order factors. In the past, the classic finite difference method has been widely used due to the rapid development of computer technology and big possibilities that this offers when solving large series of equations. This classic method, however, continued to be restricted by the enforced use of regular meshes. A finite difference discretization technique using uniform lattice spacing, and with a central second-order stepping in space and forward stepping in time, is most widely used because of its simplicity. However, as shown in Figure 2.2, after deformation, the rectangular lattices will become non-rectangular, which is not available for the classic finite difference method. Thus, we will use another finite difference method which will be discussed later.

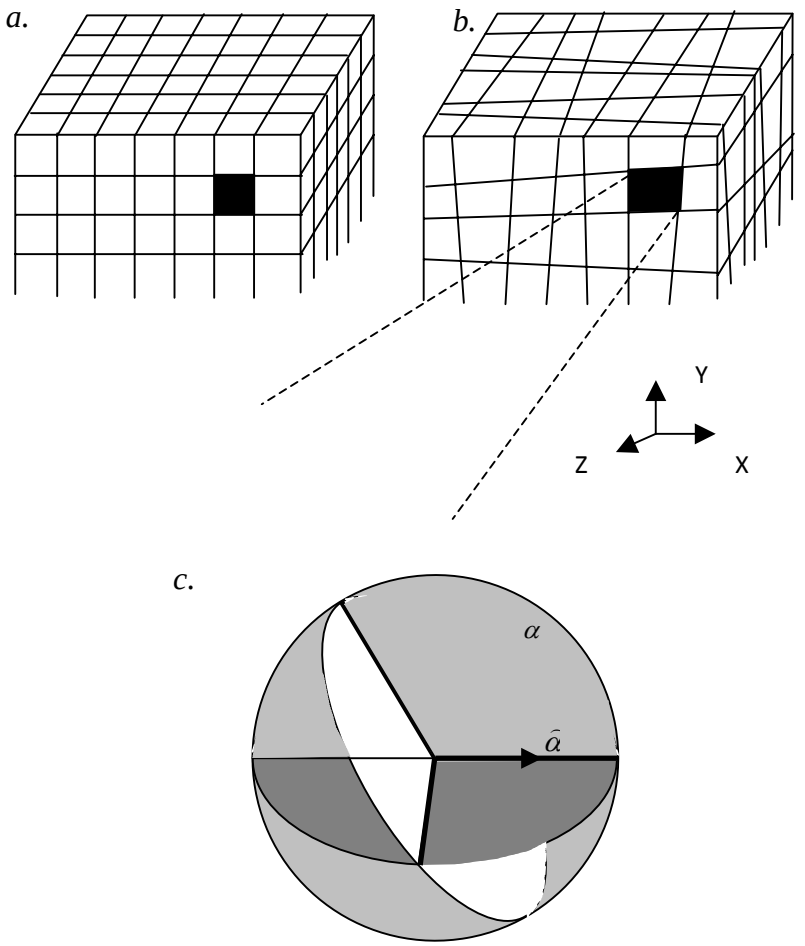

Figure 2.2: (a) Square lattices before deformation. (b) Irregular lattices during deformation. (c) Planes distortion during deformation in three-dimension.

2.3 Finite-Difference Method

2.3.1 Overview

A significant number of physical and engineering problems lead to differential equations with partial derivatives. Implicit solutions to equations of mathematical physics are obtainable only in special cases. Therefore these problems are generally solved approximately by using some numerical method. In previous work, some mathematically models integrated with the finite-element method to predict the material behaviour during deformation [28-29]. Meanwhile, another method which is one of the most universal and an effective method in wide use today for approximately solving equations is the method of finite differences.

In classical numerical techniques there are some obstacles. It may be difficult to find a simple function over the entire domain and if such functions are found they could lead to large and complicated systems of equations. However, through finite difference method, the continuous domain is replaced by a discrete set of nodes and instead of a function of continuous argument, a function of discrete arguments is considered. The value of this function is defined at the nodes of the grid or at other elements of the grid. The derivatives

entering into the differential equations and the boundary conditions are approximated by the difference expression, thus the differential problem is transformed into a system of linear or non-linear algebraic equations. Such system is often called the finite-difference scheme.

In the simulation process, the finite difference method for differential equation is carried out in the following stages. First is the writing of the finite-difference scheme which means the difference approximation to the differential equation on a grid. Second is the computer solution for difference equations, which is written in the form of a high-order system of linear or non-linear algebraic equations.

2.3.2 General finite-difference method

In finite difference method, there are two main types of scalar function of a discrete argument. In the first case, the values of the function correspond to the nodes. This is nodal discretisation. In this case, grid function u^h is a set of $M \times N$ numbers: $u^h = \left\{ u_{ij}^h, i = 1, \cdots, M; j = 1, \cdots, N \right\}$. The second possibility is cell-valued discretisation. To denote the values of a cell-valued

function, we will use the same procedure as for the mesh of a grid; that is u_{ij}^h as it is related to cell Ω_{ij}. For the cell-centred discretisation, index i varies in limits from 1 to $M-1$ and $j=1,\cdots,N-1$. Figure 2.3 explains the difference in nodal and cell-valued discretisation.

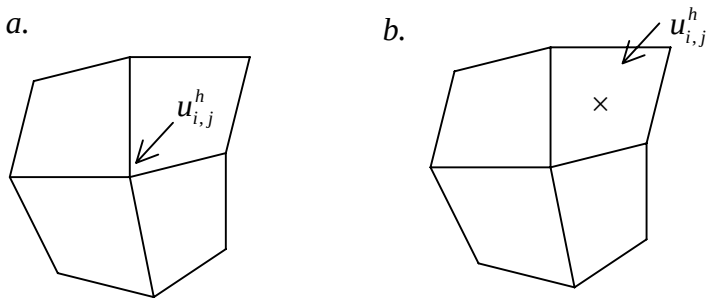

Figure 2.3: (a) Nodal discretisation; the values of function correspond to node. (b) Cell-valued discretisation; the values of the function correspond to the cell.

Take node discretisation for example and approximate the differential operator of the first partial derivative of u with respect to $\partial u/\partial x$. To construct the difference operator we will use the Green formula [25],

$$\frac{\partial u}{\partial x} = \lim_{s \to 0} \frac{\oint_l u dy}{S} \qquad (2.2)$$

where S is the area bounded by contour l. In the discrete case, the role S is played by the grid cell Ω_{ij}. Therefore l is the union of sides $l\xi_{ij}, l\eta_{i+1,j}, l\xi_{i,j+1}, l\eta_{i,j}$ as showed in Figure 2.4. For approximation of the contour integral in the right-hand side of equation (2.2), we divide the contour integral into four integral each over the corresponding side of quadrangle Ω_{ij} and for the approximate evaluation of each integral, we use the trapezium rule. As a result, we obtain the following expression for the difference analog of derivative $\partial u / \partial x$:

$$(D_x u^h)_{ij} = \frac{(u_{i+1,j+1} - u_{i,j})(y_{i,j+1} - y_{i+1,j}) - (u_{i,j+1} - u_{i+1,j})(y_{i+1,j+1} - y_{i,j})}{2\Omega_{ij}}$$

(2.3)

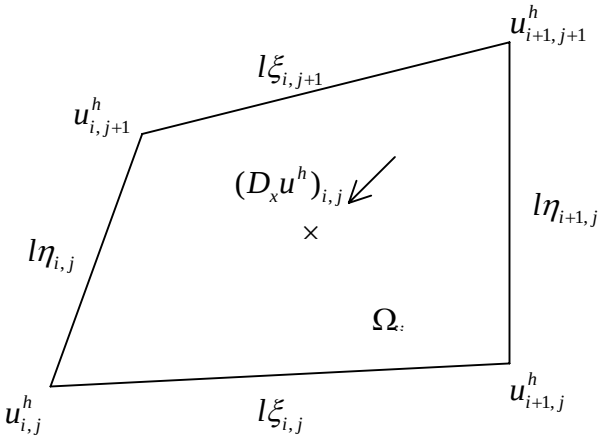

Figure 2.4: Stencil for operator D_x

In the example of D_x we can demonstrate the notion stencil of difference operators in 2-D. The stencil is a set of nodes that participate in the formula for discrete operators. Therefore, the stencil of operator D_x in cell (i, j) contains nodes $(i, j), (i+1, j), (i+1, j+1), (i, j+1)$.

2.3.3 Application of finite-difference method

The finite difference method is a technique used principally for

solving partial differential equation approximately. The method is not synonymous with any physical theory, although its heaviest use probably has been in solid and structural mechanics. While there are a few features common to all finite difference formulation, there is no single universal formulation. Rather, there is considerable variety in the implementations of the method, usually motivated by aspects of the system of equations being solved.

In the simulation, the direction of each plane in the classical phase-field model will be changed because of the homogeneous deformation. Figure 2.2 schematically shows how meshes are changed during deformation process. Figure 2.5 shows directions of each plane from one random point in three dimension and Figure 2.6, Figure 2.7 and Figure 2.8 show the lattices evolution in the three directions during deformation.

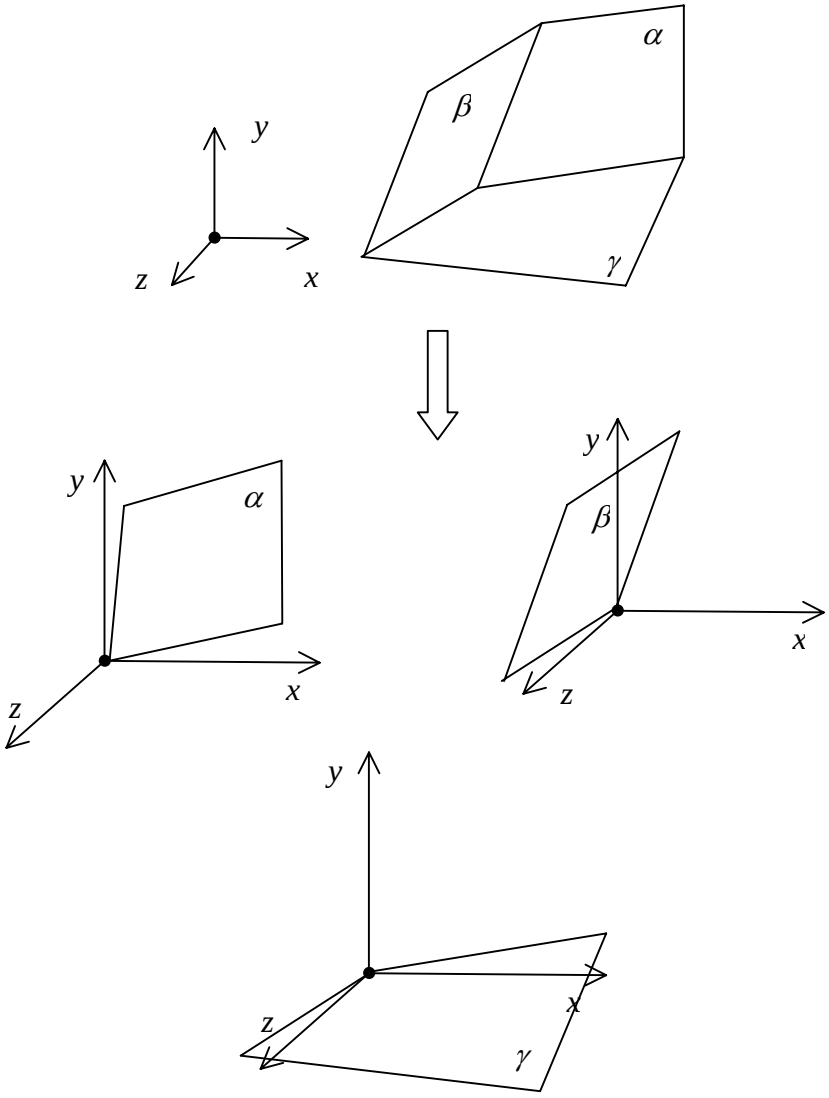

Figure 2.5: Direction of each plane from one random point in the lattices.

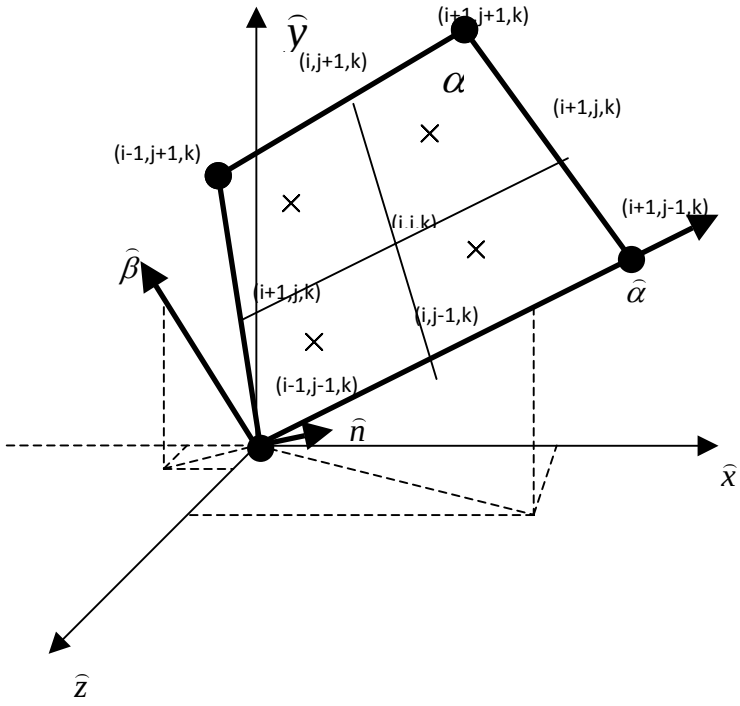

Figure 2.5: The irregular lattices in α plane during deformation.

Nevertheless, considering α plane in three dimensions, based on irregular lattices as showed in Figure 2.5 and finite difference method, we can get the formula

In α plane:

$$\frac{\partial \phi_{i,j,k}}{\partial \alpha} = \frac{1}{2\Omega_\alpha}\left[(\phi_{i,j+1,k} - \phi_{i,j-1,k})(\beta_{i-1,j,k} - \beta_{i+1,j,k}) - (\phi_{i-1,j,k} - \phi_{i+1,j,k})(\beta_{i,j+1,k} - \beta_{i,j-1,k})\right]$$

(2.4)

$$\frac{\partial^2 \phi_{i,j,k}}{\partial \alpha^2} = \frac{1}{2\Omega'_\alpha}[(\frac{\partial \phi_{(i+1,j+1,k)}}{\partial \alpha} - \frac{\partial \phi_{(i-1,j-1,k)}}{\partial \alpha})(\beta_{(i-1,j+1,k)} - \beta_{(i+1,j-1,k)})$$

$$-(\frac{\partial \phi_{(i-1,j+1,k)}}{\partial \alpha} - \frac{\partial \phi_{(i+1,j-1,k)}}{\partial \alpha})(\beta_{(i+1,j+1,k)} - \beta_{(i-1,j-1,k)})]$$

(2.5)

$$\frac{\partial^2 \phi_{i,j,k}}{\partial \alpha \partial \beta} = \frac{1}{2\Omega'_\alpha}[(\frac{\partial \phi_{(i+1,j+1,k)}}{\partial \beta} - \frac{\partial \phi_{(i-1,j-1,k)}}{\partial \beta})(\beta_{(i-1,j+1,k)} - \beta_{(i+1,j-1,k)})$$

$$-(\frac{\partial \phi_{(i-1,j+1,k)}}{\partial \beta} - \frac{\partial \phi_{(i+1,j-1,k)}}{\partial \beta})(\beta_{(i+1,j+1,k)} - \beta_{(i-1,j-1,k)})]$$

(2.6)

where Ω_α is the area of quadrangle which connect points $(i, j+1, k), (i, j-1, k), (i+1, j, k)$ and $(i-1, j, k)$. Ω'_α is the area of quadrangle which connect points $(i+1, j+1, k), (i-1, j+1, k), (i+1, j-1, k)$ and $(i-1, j-1, k)$ in Figure 2.5.

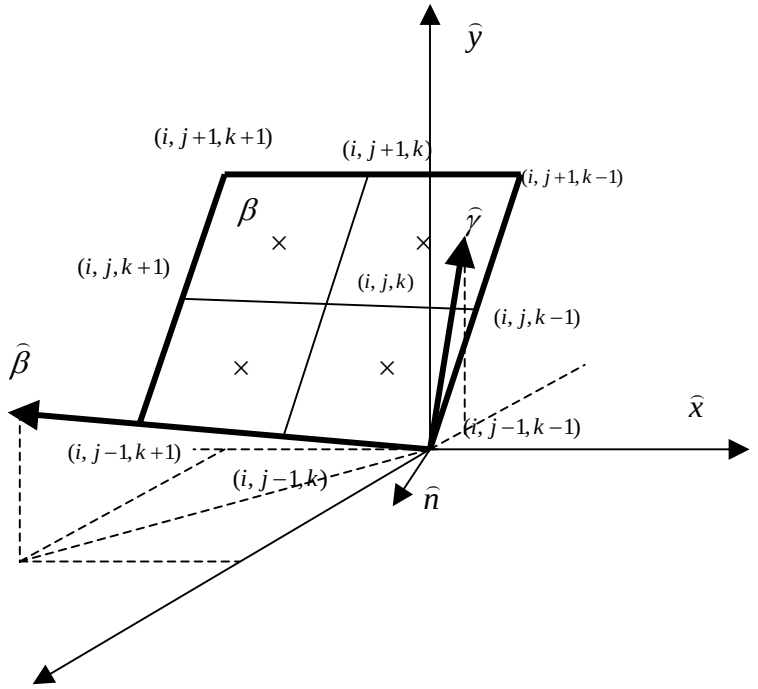

Figure 2.6: The irregular lattices in β plane during deformation.

In β plane:

$$\frac{\partial \phi_{i,j,k}}{\partial \beta} = \frac{1}{2\Omega_\beta}\left[(\phi_{i,j+1,k} - \phi_{i,j-1,k})(\gamma_{i,j,k+1} - \gamma_{i,j,k-1}) - (\phi_{i,j,k+1} - \phi_{i,j,k-1})(\gamma_{i,j+1,k} - \gamma_{i,j-1,k})\right]$$

(2.7)

$$\frac{\partial^2 \phi_{i,j,k}}{\partial \beta^2} = \frac{1}{2\Omega'_\beta}[(\frac{\partial \phi_{(i,j+1,k+1)}}{\partial \beta} - \frac{\partial \phi_{(i,j-1,k-1)}}{\partial \beta})(\gamma_{(i,j+1,k-1)} - \gamma_{(i,j-1,k+1)})$$

$$+(\frac{\partial \phi_{(i,j+1,k-1)}}{\partial \beta}-\frac{\partial \phi_{(i,j-1,k+1)}}{\partial \beta})(\alpha_{(i,j+1,k+1)}-\alpha_{(i,j-1,k-1)})]$$

(2.8)

$$\frac{\partial^2 \phi_{i,j,k}}{\partial \beta \partial \gamma}=\frac{1}{2\Omega'_{\beta}}[(\frac{\partial \phi_{(i,j+1,k+1)}}{\partial \beta}-\frac{\partial \phi_{(i,j-1,k-1)}}{\partial \beta})(\beta_{(i,j+1,k-1)}-\beta_{(i,j-1,k+1)})$$

$$-(\frac{\partial \phi_{(i,j+1,k-1)}}{\partial \beta}-\frac{\partial \phi_{(i,j-1,k+1)}}{\partial \beta})(\beta_{(i,j+1,k+1)}-\beta_{(i,j-1,k-1)})]$$

(2.9)

where Ω_{β} is the area of quadrangle which connect points $(i, j+1, k), (i, j-1, k), (i, j, k+1)$ and $(i, j, k-1)$. Ω'_{β} is the area of quadrangle which connect points $(i, j+1, k+1), (i, j-1, k-1), (i, j+1, k-1)$ and $(i, j-1, k+1)$ in Figure 2.6

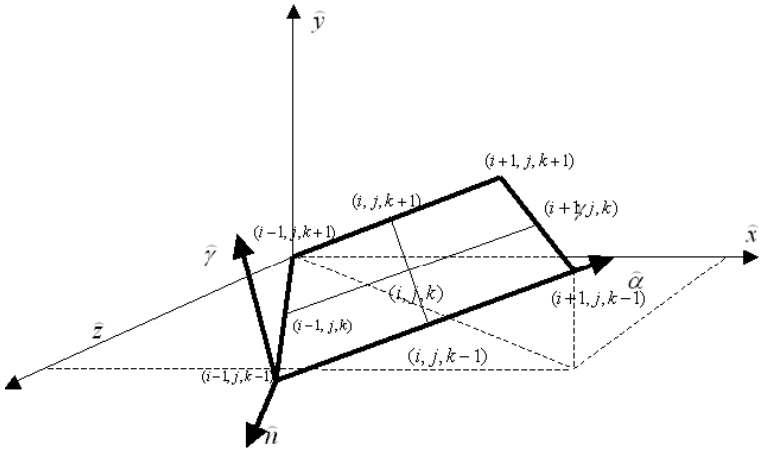

Figure 2.7: The irregular lattices in γ plane during deformation.

In γ plane:

$$\frac{\partial \phi_{i,j,k}}{\partial \gamma} = \frac{1}{2\Omega_\gamma}\left[(\phi_{i,j,k+1} - \phi_{i,j,k-1})(\alpha_{i-1,j,k} - \alpha_{i+1,j,k}) + (\phi_{i-1,j,k} - \phi_{i+1,j,k})(\alpha_{i,j,k+1} - \alpha_{i,j,k-1})\right]$$

(2.10)

$$\frac{\partial^2 \phi_{i,j,k}}{\partial \gamma^2} = \frac{1}{2\Omega'_\gamma}[(\frac{\partial \phi_{(i+1,j,k+1)}}{\partial \gamma} - \frac{\partial \phi_{(i-1,j,k-1)}}{\partial \gamma})(\alpha_{(i-1,j,k+1)} - \alpha_{(i+1,j,k-1)})$$

$$+(\frac{\partial \phi_{(i-1,j,k+1)}}{\partial \gamma} - \frac{\partial \phi_{(i+1,j,k-1)}}{\partial \gamma})(\alpha_{(i+1,j,k+1)} - \alpha_{(i-1,j,k-1)})]$$

(2.11)

$$\frac{\partial^2 \phi_{i,j,k}}{\partial \alpha \partial \gamma} = \frac{1}{2\Omega'_\gamma}[(\frac{\partial \phi_{(i+1,j,k+1)}}{\partial \gamma} - \frac{\partial \phi_{(i-1,j,k-1)}}{\partial \gamma})(\gamma_{(i-1,j,k+1)} - \gamma_{(i+1,j,k-1)})$$

$$-(\frac{\partial \phi_{(i-1,j,k+1)}}{\partial \gamma} - \frac{\partial \phi_{(i+1,j,k-1)}}{\partial \gamma})(\gamma_{(i+1,j,k+1)} - \gamma_{(i-1,j,k-1)})]$$

(2.12)

where Ω_γ is the area of quadrangle which connect points $(i, j, k+1), (i, j, k-1), (i-1, j, k)$ and $(i+1, j, k)$. Ω'_γ is the area of quadrangle which connect points $(i+1, j, k+1), (i+1, j, k-1), (i-1, j, k-1)$ and $(i-1, j, k+1)$ in

Figure 2.6

These formulas are for cell-centred discretisation and they refer to a group of established nodes related to one, which is denoted as central node. For calculating the value of one point, we have to use 21 neighbouring points. Actually, there is no best method way for obtaining approximating difference formulae, and as many different methods as possible will be tested. The only requirement is that the formula, having been obtained, must pass certain test of accuracy, consistency, stability and convergence.

During deformation, each quadrangle will probably have different shape. For the purpose of the program we define a set of parameters for viewing arbitrary planes through deformation, which is easy to visualize for the user. Therefore, we have to use coordinate transformation to make all the phase-field governing equation of each point can be explained in one coordinate.

2.4 Coordinate transformation

2.4.1 General coordinate transformation

The need for the use of more than one coordinate system comes from the fact that many different physical phenomena are easier calculated or understood in a system that is appropriate for the phenomenon. Frequently, it is quite necessary to transform from one coordinate system to another.

For the definition of a coordinate system in three-dimensional space, one has only to specify the direction of one of the axes, and the orientation of one of the other axes in the plane perpendicular to this direction. The third axis follows automatically in order to complete a right-handed orthogonal set. As showed in Figure 2.5, $\hat{\alpha}$ means the direction along the irregular lattices. $\hat{\beta}$ is perpendicular to $\hat{\alpha}$ and $\hat{n}$ is the normal direction of α plane which means a random plane in the model. The coordinate systems and transformations used in this simulation are Cartesian coordinates system.

In Cartesian coordinate system, a position vector $\vec{M}$ in a three-dimensional space can be represented in vector form as

$$r_m = \overline{O_m M} = x_m i_m + y_m j_m + z_m k_m \qquad (2.13)$$

where (i_m, j_m, k_m) are the unit vectors of coordinate axes, and by the

column matrix it can written as:

$$r_m = \begin{bmatrix} x_m \\ y_m \\ z_m \end{bmatrix} \qquad (2.14)$$

The subscript m indicates that the position vector is represented in coordinate system $S_m(x_m, y_m, z_m)$. There are many ways to define an arbitrary rotation, scaling and translation of one coordinate frame into another. Consider two coordinate systems $S_m(x_m, y_m, z_m)$ and $S_n(x_n, y_n, z_n)$ as an example. Point M is represented in coordinate system S_m by the position vector as:

$$r_m = \begin{bmatrix} x_m & y_m & z_m & 1 \end{bmatrix}^T \qquad (2.15)$$

In coordinate system S_n the same point can be determined by the position vector as:

$$r_n = \begin{bmatrix} x_n & y_n & z_n & 1 \end{bmatrix}^T \qquad (2.16)$$

with the matrix equation:

$$r_n = M_{nm} r_m \quad (2.17)$$

Matrix M_{nm} is represented by:

$$M_{nm} = \begin{bmatrix} a_{11} & a_{12} & a_{13} & a_{14} \\ a_{21} & a_{22} & a_{23} & a_{24} \\ a_{31} & a_{32} & a_{33} & a_{34} \\ 0 & 0 & 0 & 1 \end{bmatrix}$$

$$= \begin{bmatrix} (i_n \cdot i_m) & (i_n \cdot j_m) & (i_n \cdot k_m) & (\overline{O_n O_m} \cdot i_n) \\ (j_n \cdot i_m) & (j_n \cdot j_m) & (j_n \cdot k_m) & (\overline{O_n O_m} \cdot j_n) \\ (k_n \cdot i_m) & (k_n \cdot j_m) & (k_n \cdot k_m) & (\overline{O_n O_m} \cdot k_n) \\ 0 & 0 & 0 & 1 \end{bmatrix}$$

$$= \begin{bmatrix} \cos(\widehat{x_n, x_m}) & \cos(\widehat{x_n, y_m}) & \cos(\widehat{x_n, z_m}) & x_n^{(O_m)} \\ \cos(\widehat{y_n, x_m}) & \cos(\widehat{y_n, y_m}) & \cos(\widehat{y_n, z_m}) & y_n^{(O_m)} \\ \cos(\widehat{z_n, x_m}) & \cos(\widehat{z_n, y_m}) & \cos(\widehat{z_n, z_m}) & z_n^{(O_m)} \\ 0 & 0 & 0 & 1 \end{bmatrix}$$

(2.18)

Here, (i_n, j_n, k_n) are the unit vectors of the axes of the new coordinate system; (i_m, j_m, k_m) are the unit vectors of the axes of the original coordinate system; O_n and O_m are the origins of the

new and original coordinate systems; subscript nm in the designation M_{nm} indicates that the coordinate transformation is performed from S_m to S_n. The determination of elements $a_{lk}(k=1,2,3,4; l=1,2,3)$ of matrix M_{nm} is based on the following rules. Firstly elements of the 3×3 submatrix

$$L_{nm}=\begin{bmatrix} a_{11} & a_{12} & a_{13} \\ a_{21} & a_{22} & a_{23} \\ a_{31} & a_{32} & a_{33} \end{bmatrix} \qquad (2.19)$$

represents the direction cosines of the original unit vectors (i_m, j_m, k_m) in the new coordinate system S_n. The number l indicates the original coordinate axis and the number k indicates the new coordinate axis. Axes x, y, z are given number 1, 2 and 3, respectively. Elements a_{14}, a_{14} and a_{34} represent the new coordinates $x_n^{(O_m)}, y_n^{(O_m)}, z_n^{(O_m)}$ of the original O_m.

2.4.2 Application of coordinate transformation

Using the coordinate transformation rule discussed above and taking

α plane as an example, we can get:

$$\hat{\alpha} = \frac{(x_{i+1,j,k} - x_{i,j,k})\hat{x} + (y_{i+1,j,k} - x_{i,j,k})\hat{y} + (z_{i+1,j,k} - z_{i,j,k})\hat{z}}{\left|\alpha_{i+1,j,k} - \alpha_{i,j,k}\right|^2} \qquad (2.20)$$

$$\hat{\beta} = \frac{\hat{\alpha} \times \hat{n}}{\left|\beta_{i+1,j,k} - \beta_{i,j,k}\right|^2} \qquad (2.21)$$

According the equations (2.17) and (2.18), the relationships between these transformations are found by directly comparison of the transformation matrix elements:

$$\begin{pmatrix} \partial\alpha \\ \partial\beta \\ \partial n \end{pmatrix} = \begin{pmatrix} i_x \cdot i_\alpha & i_y \cdot j_\alpha & i_z \cdot k_\alpha \\ j_x \cdot i_\beta & j_y \cdot j_\beta & j_z \cdot k_\beta \\ k_x \cdot i_n & k_y \cdot j_n & k_z \cdot k_n \end{pmatrix} \begin{pmatrix} \partial x \\ \partial y \\ \partial z \end{pmatrix} \qquad (2.22)$$

where i_x, i_y and i_z are the unit vectors of the XYZ system, and i_α, i_β and i_n are the unit vectors of the $\alpha\beta n$ system.

Furthermore, in XYZ system, the first order partial derivatives were discretized by using

$$\begin{pmatrix} \frac{\partial \phi}{\partial x} \\ \frac{\partial \phi}{\partial y} \\ \frac{\partial \phi}{\partial z} \end{pmatrix} = \begin{pmatrix} \frac{\partial \alpha}{\partial x} & \frac{\partial \beta}{\partial x} & \frac{\partial n}{\partial x} \\ \frac{\partial \alpha}{\partial y} & \frac{\partial \beta}{\partial y} & \frac{\partial n}{\partial y} \\ \frac{\partial \alpha}{\partial z} & \frac{\partial \beta}{\partial z} & \frac{\partial n}{\partial z} \end{pmatrix} \begin{pmatrix} \frac{\partial \phi}{\partial \alpha} \\ \frac{\partial \phi}{\partial \beta} \\ \frac{\partial \phi}{\partial n} \end{pmatrix} \qquad (2.23)$$

$$\frac{\partial \phi}{\partial n} = 0 \qquad (2.24)$$

According to the nodes in the cell we want to get discretation value and the lattices geometry, using equations discussed above, we can derive the formula for operator $\frac{\partial \phi_{i,j,k}}{\partial x}$, $\frac{\partial \phi_{i,j,k}}{\partial y}$, $\frac{\partial \phi_{i,j,k}}{\partial z}$, $\frac{\partial^2 \phi_{i,j,k}}{\partial x^2}$, $\frac{\partial^2 \phi_{i,j,k}}{\partial y^2}$, $\frac{\partial^2 \phi_{i,j,k}}{\partial z^2}$, $\frac{\partial^2 \phi_{i,j,k}}{\partial xy}$, $\frac{\partial^2 \phi_{i,j,k}}{\partial yz}$ and $\frac{\partial^2 \phi_{i,j,k}}{\partial xz}$ in the similar way by using the 21-neighbor points and geometry of the cell in three dimensions.

2.5 Conclusion

All spatial derivatives in phase-field governing equation were discretized using finite difference formulas that we generalized above. (i, j, k) denotes the position of the node along the $\hat{x}, \hat{y}$ and $\hat{z}$ axes, respectively. The second order partial derivatives were

discretized using the nine-point formula. Time stepping was done using a first-order Euler scheme.

From the above discussion, it may be seen that using finite difference method and coordinate transformation method on phase-field model depends on the following factors:

a. The position of nodes. This underlines the great importance of the selection of nodes of the lattices. The selection or placement of the nodes has a great influence on the results. Normally, when selecting the nodes surrounding the central node, we selected those closest to the central one in the Cartesian coordinates.
b. The relative coordinate of the lattice spacing. This is more important in heterogeneous deformation because the neighbour lattice maybe undergo deformation in different directions.

Chapter 3

Simulation and discussion

3.1 Overview

Ideally, in an attempt to reduce experimental costs improve the understanding of the mechanism, one would like to make a prediction of a new material's behaviour by numerical simulation, with the primary goal being to accelerate trial and error experimental testing. Simulation raises the possibility that modern numerical methods can play a significant role in analysis of microstructure evolution.

3.2 Simulation

3.2.1 System diagram

According to the numerical procedures, which were discussed in chapter 2, we can get the results of the simulation. As described in chapter 1, there are four main types of homogeneous deformations. And in this numerical simulation, we combined phase-field model with simple shear deformation together. According to Table 1.2 which shows different value of S matrix, during simple shear deformation, $S_{11} = S_{22} = S_{33} = 1$, S_{13} is the shear value, and all the other elements of S are zero. Furthermore, for simplicity and to ensure mechanical equilibrium, we assume uniform density and temperature throughout the system and that there is no mass and temperature diffusion in the phase.

As discussed in chapter 2, Figure 3.1 is the system diagram.

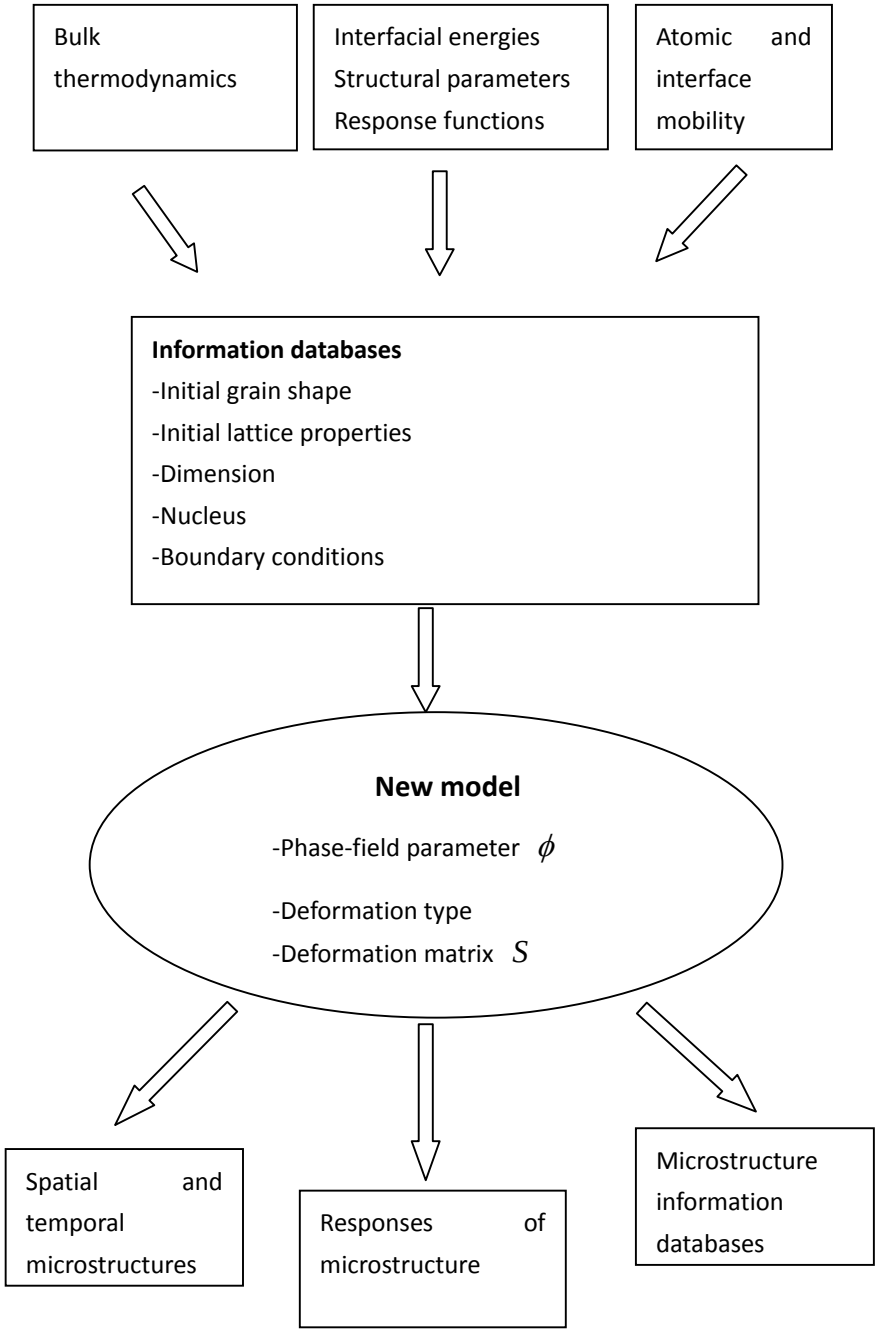

Figure 3.1: System diagram of whole simulation

3.2.2 Parameters of simulation

The simulations were performed on a cubic grid of size $N_1 \times N_2 \times N_3 = 160 \times 160 \times 120$ with initial constant grid spacing. Simulations were started with a small spherical seed in the corner of the cubic. After deformation, lattices geometry such as grid spacing is not constant anymore.

The phase-field governing equation contains many phenomenological parameters, which are difficult to determine for real alloys. In this simulation, the thermodynamic data for the martenstic transition of Fe_0.4wt%C steel at $250^{\circ}\mathrm{C}$ is used. In metallic materials the thickness of interface is about 3 to 5 atomic distances which is about 1 nm but in this model the half thickness of the interface is chosen as 14.3nm to accelerate the simulation without losing much details of the grain morphology. The lattice distance was chosen as $\Delta x = 7.15\mathrm{nm}$ so that there are four grids across the interfaces. According to the MTDATA thermodynamic database, bulk free energy $g_0 = -1.73 \times 10^9\,\mathrm{J/m^2}$ and $g_1 = -2.09 \times 10^9\,\mathrm{J/m^2}$. The interface energy is $800\mathrm{erg/cm^2}$ [26].

Three sets of anisotropy coefficients are applied in the simulation, as list in Table 3.1. Figure 3.1 demonstrates the three different grain

morphology without deformation using different interface anisotropy in Table 3.1.

	Case A	Case B	Case C
k_1	-0.863	0.402	0.0
k_2	0.395	0.00144	0.0
k_3	0.0238	0.00066	0.0

Table 3.1: Different sets of anisotropic coefficients

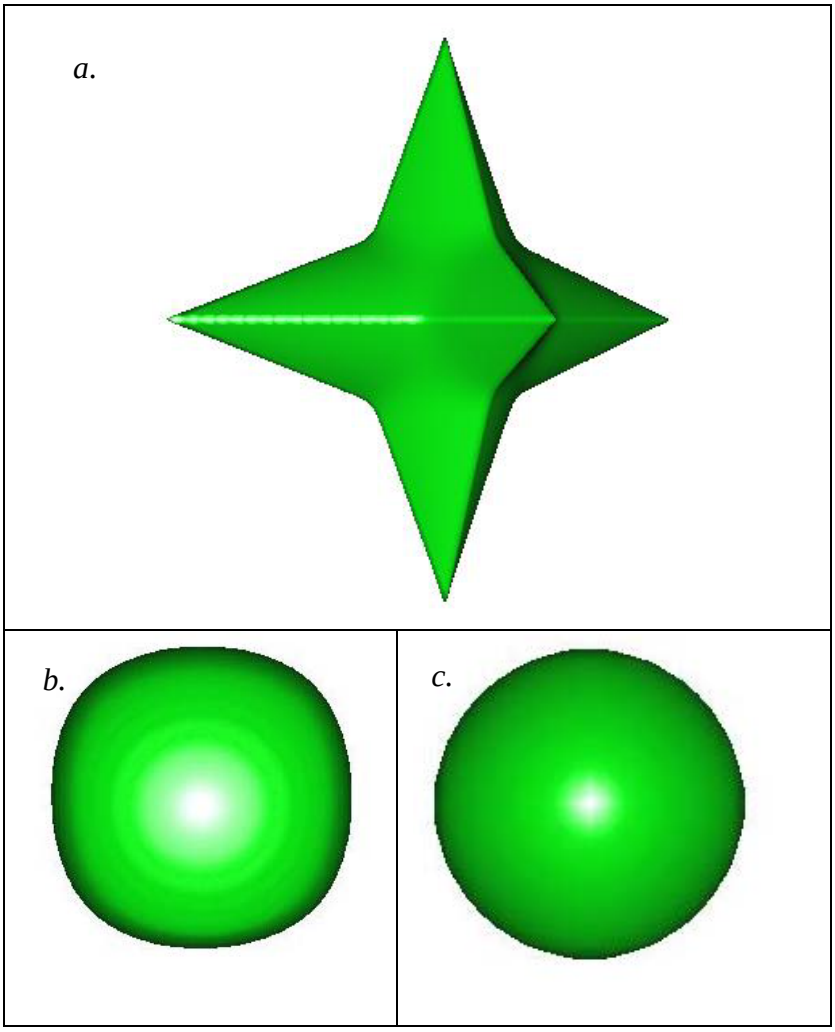

Figure 3.1 Grain morphology at 5000 time steps under different interface anisotropy list in Table 3.1. (a) Case A, (b) Case B and (c) Case C.

3.2.3 Results

Figure 3.2, 3.4 and 3.6 show the microstructure evolution in three different sets of anisotropy parameters. Three types of different grain growth under each anisotropic parameter are simulated. One is normal grain growth without deformation. The second is simple shear deformation along the $\hat{y}$-axis after grain growth. The third is the grain growth while undergoing homogeneous deformation along the $\hat{y}$-axis.

Figure 3.3, 3.5 and 3.7 show microstructure evolution in different time steps while undergoing simple shear deformation using three different anisotropy parameters.

Case A (Dendrite)

Without deformation; time steps=12000
a. 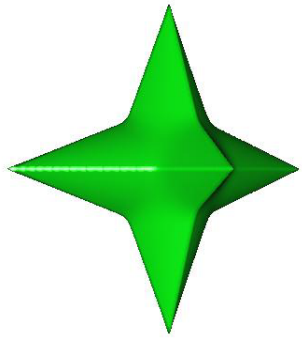
Deformation after grain growth; time steps=12000
b. 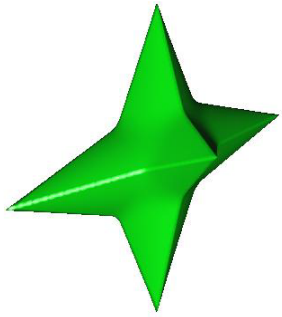
Deformation during grain growth; time steps=12000
c.

Figure 3.2: Grain morphology at $M_{\phi}=100$ computation using anisotropy coefficient in Case A: (a) No simple shear deformation; (b) With simple shear deformation after grain growth for 12000 time

steps; (c) After 12000 time steps with simple shear deformation in every 6000 time steps while grain growth.

Case A (Dendrite)

Time steps=6000	Time steps=8000
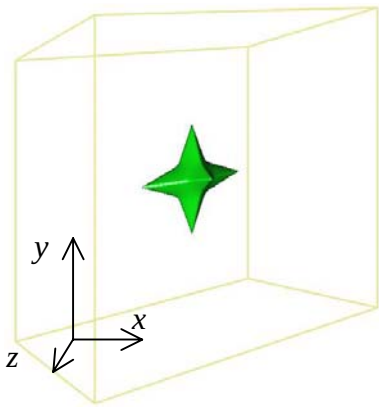	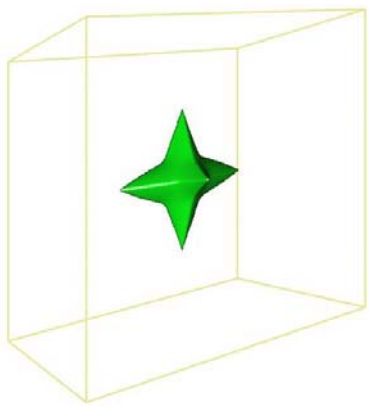
Time steps=10000	Time steps=12000
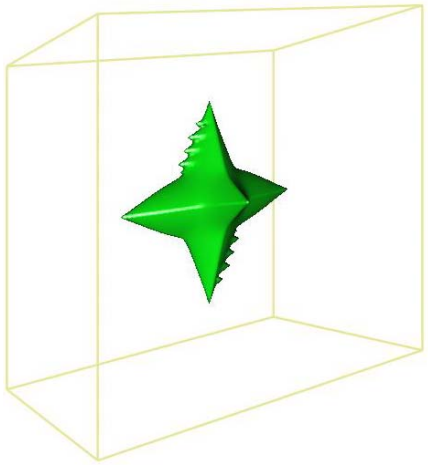	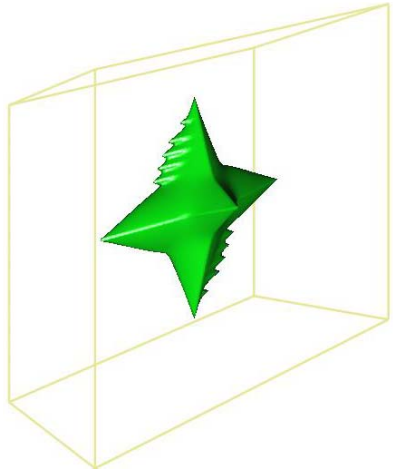

Time steps=14000	Time steps=16000
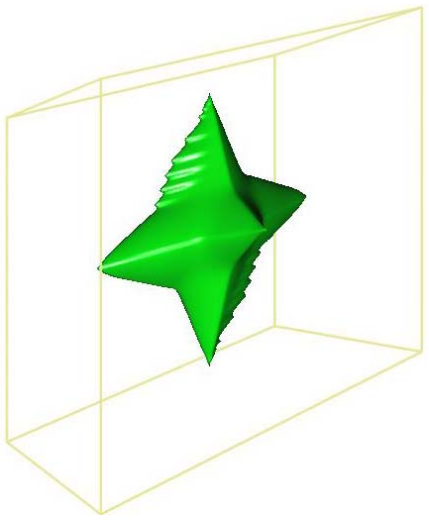	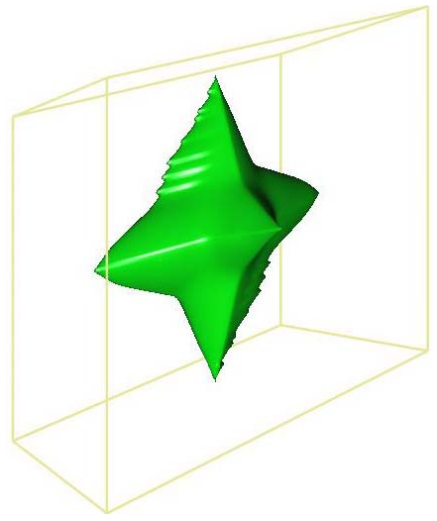

Figure 3.3: Case A: Grain morphology at $M_{\phi} = 100$ computation: Microstructure evolution during simple shear deformation in different time steps.

Case B (Cubic)

Without deformation	
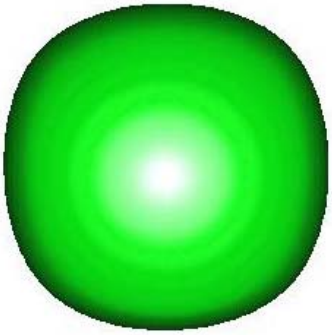	
Deformation after grain growth; time steps=18000	Deformation during grain growth; time steps=18000
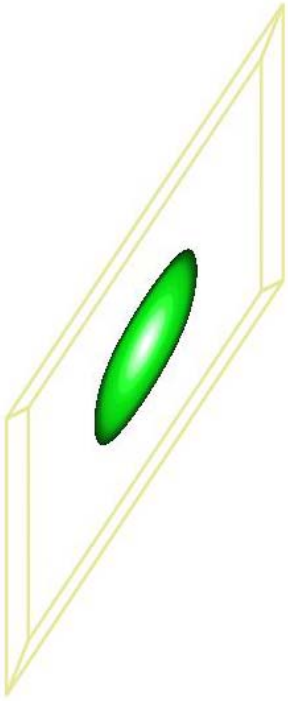	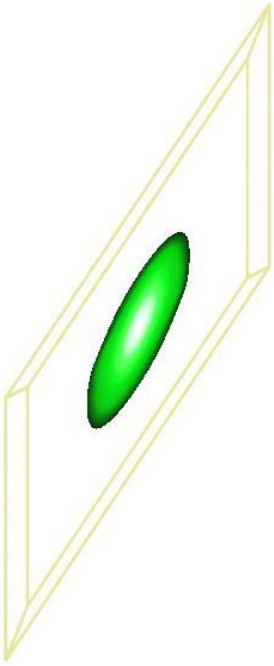

Figure 3.4: Grain morphology at $M_{\phi} = 100$ computation using

anisotropy coefficient in Case B: (a) No simple shear deformation; (b) With simple shear deformation after grain growth for 18000 time steps; (c) After 18000 time steps with simple shear deformation in every 6000 time steps while grain growth.

Case B (Cubic)

Time steps=4000	Time steps=6000
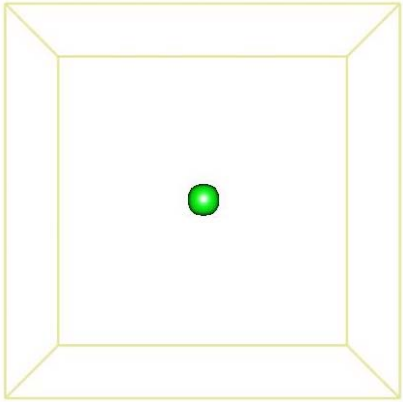	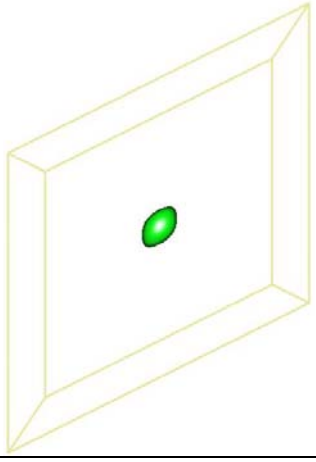

Time steps=10000	Time steps=12000
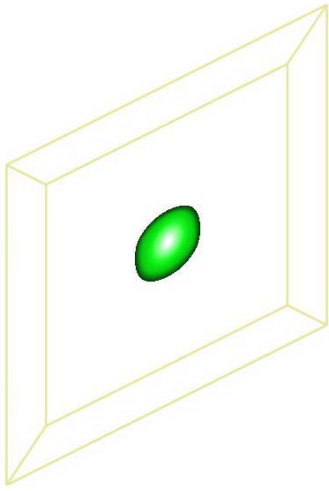	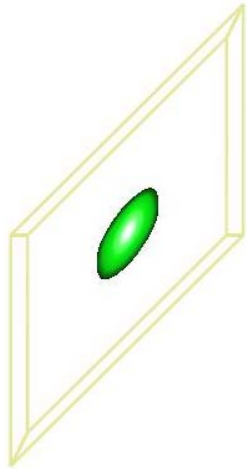
Time steps=16000	Time steps=18000
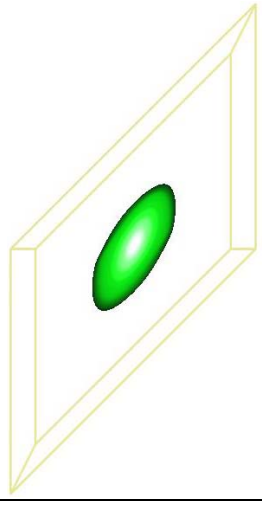	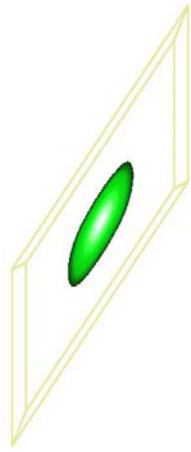

Figure 3.5: Case B: Grain morphology at $M_{\phi} = 100$ computation: Microstructure evolution during simple shear deformation in different time steps.

Case C (Isotropy)

Without deformation	
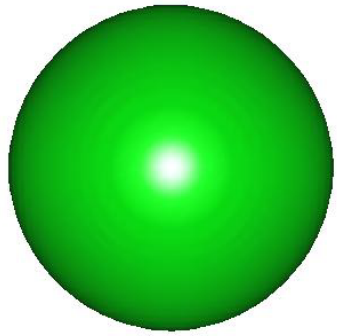	
Deformation after grain growth; time steps=12000	Deformation during grain growth; time steps=18000
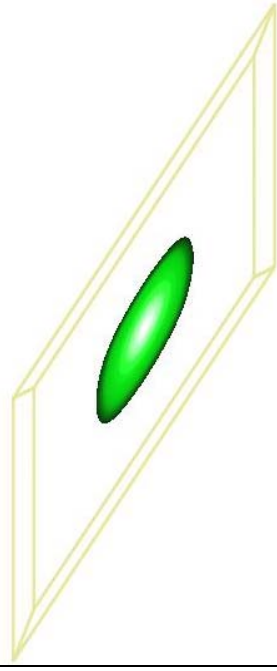	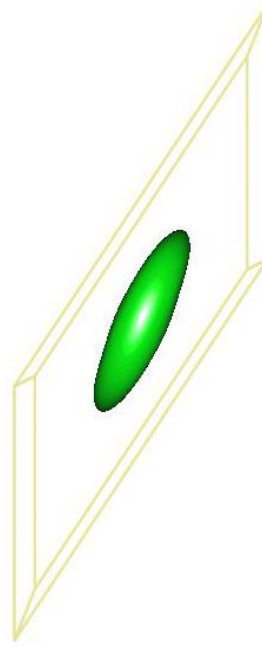

Figure 3.6: Grain morphology at $M_{\phi}=100$ computation using anisotropy coefficient in Case C: (a) No simple shear deformation; (b) With simple shear deformation after grain growth for 18000 time

steps; (c) After 18000 time steps with simple shear deformation in every 6000 time steps while grain growth.

Case C (Isotropy)

Time steps=4000	Time steps=6000
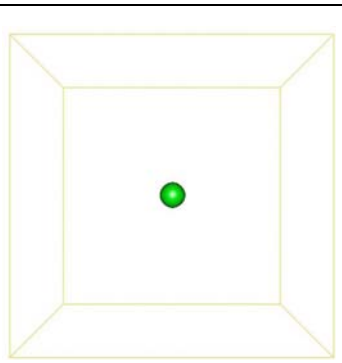	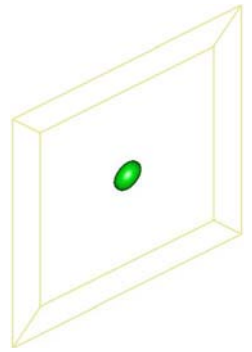
Time steps=10000	Time steps=12000
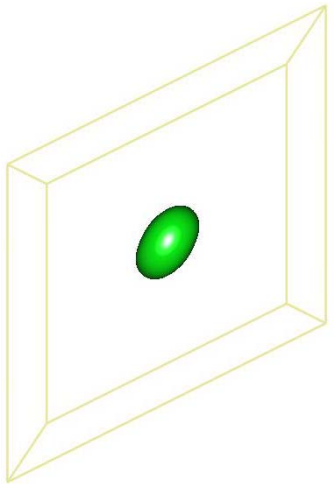	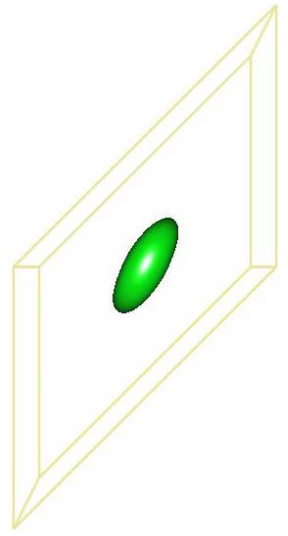

Time steps=16000	Time steps=18000
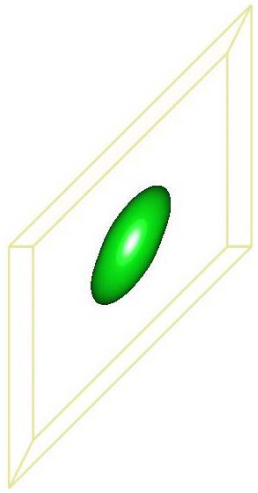	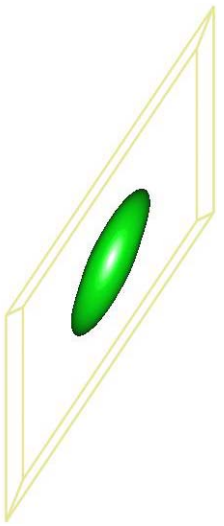

Figure 3.7: Case C: Grain morphology at $M_{\phi} = 100$ computation: Microstructure evolution during simple shear deformation in different time steps.

3.3 Discussion

As demonstrated earlier, three different processing bring out three different microstructure evolutions and the morphology of the growing grain presents here to minimize the free energy of the whole system. In addition, after a particular time step, the new

microstructure disappears step by step which because of the effect of grain growth rate is more effective than the effect of the change in normal interface vector.

In solid state, the interactions between atoms in crystal are stronger. Thus the atoms are able to move only in vibrations of extremely low amplitude about fixed positions relative to one another. As a result, solids have rigidity, fixed shape, and mechanical strength. Furthermore, when a force of any magnitude is applied to a solid body the body becomes distorted; that is, some part of the body moves with respect to some neighbouring portion. As a result of this displacement the atomic attractive forces in the body set up restoring forces that resist the alteration and tend to restore the body to its original shape. The restoring force in a deformed body is termed stress and has the units of force per area. The dimensional change produced by an applied force is called strain.

One effect of simple shear deformation on microstructure evolution is the direct grain distortion which will change the grain size and grain size distribution in phase transformation. Subsequently, this will change the grain interface orientation and normal vector $\hat{n}$ as showed in Figure 3.8.

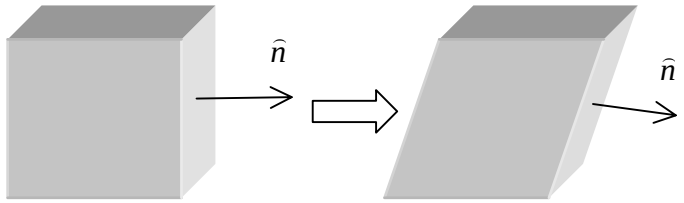

Figure 3.8: schematic diagram of interface orientation evolution during deformation.

The normal direction of grain interface $\hat{n}$ is related with the anisotropy surface energy in equation (1.12). Furthermore, it will change the grain interface migration pattern and eventually lead to the change of grain morphology compared with deformation after phase transformation.

To more specifically explain this phenomenon, we assuming an operator G to represent the grain growth in Cartesian coordinates:

$$G(\hat{n}) = \left[G_x(\hat{n}) \quad G_y(\hat{n}) \quad G_z(\hat{n}) \right] \quad (3.1)$$

Grain growth in phase transition while undergoing deformation can be described:

$$G_{total} = S_{ij} \cdot \sum_{t=o}^{t} G_i(\hat{n}) \quad (3.2)$$

where G_i means grain growth matrix after i th deformation.

Meanwhile, grain growth in phase transition before deformation:

$$G'_{total} = \sum_{t=o}^{t} [G(\hat{n})S_{ij}] \quad (3.3)$$

Because the normal unit vector of interface $\hat{n}$ is related to the deformation operator S_{ij}, so

$$G_{total} \neq G'_{total} \quad (3.4)$$

when the anisotropic effect of interface is ignored, $G_{total} = G'_{total}$. Therefore, from the equations discussed above, it is reasonable that the microstructure obtain by phase transition during deformation can been completely different from that deformation after phase transiton.

Figure 3.9 describes the whole change of lattices in three different situations. One is normal grain growth without deformation. Second one is simple shear deformation along the $\hat{y}$-axis after grain growth. The last one is grain growth while undergoing homogeneous deformation along the $\hat{y}$-axis. Figure 3.10, 3.11 and 3.12 show the cross-section of grain growth in phase transition during deformation and after deformation along three axes.

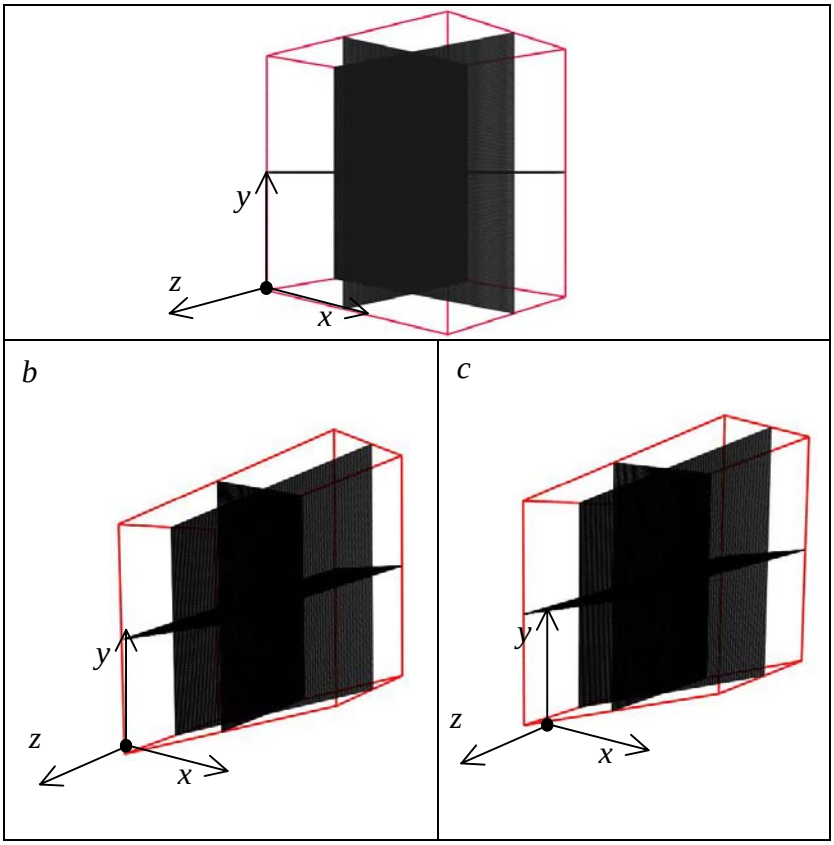

Figure 3.9: Distortion of the whole unit cell. (a) No deformation. (b) Deformation during grain growth. (c) Deformation after grain growth.

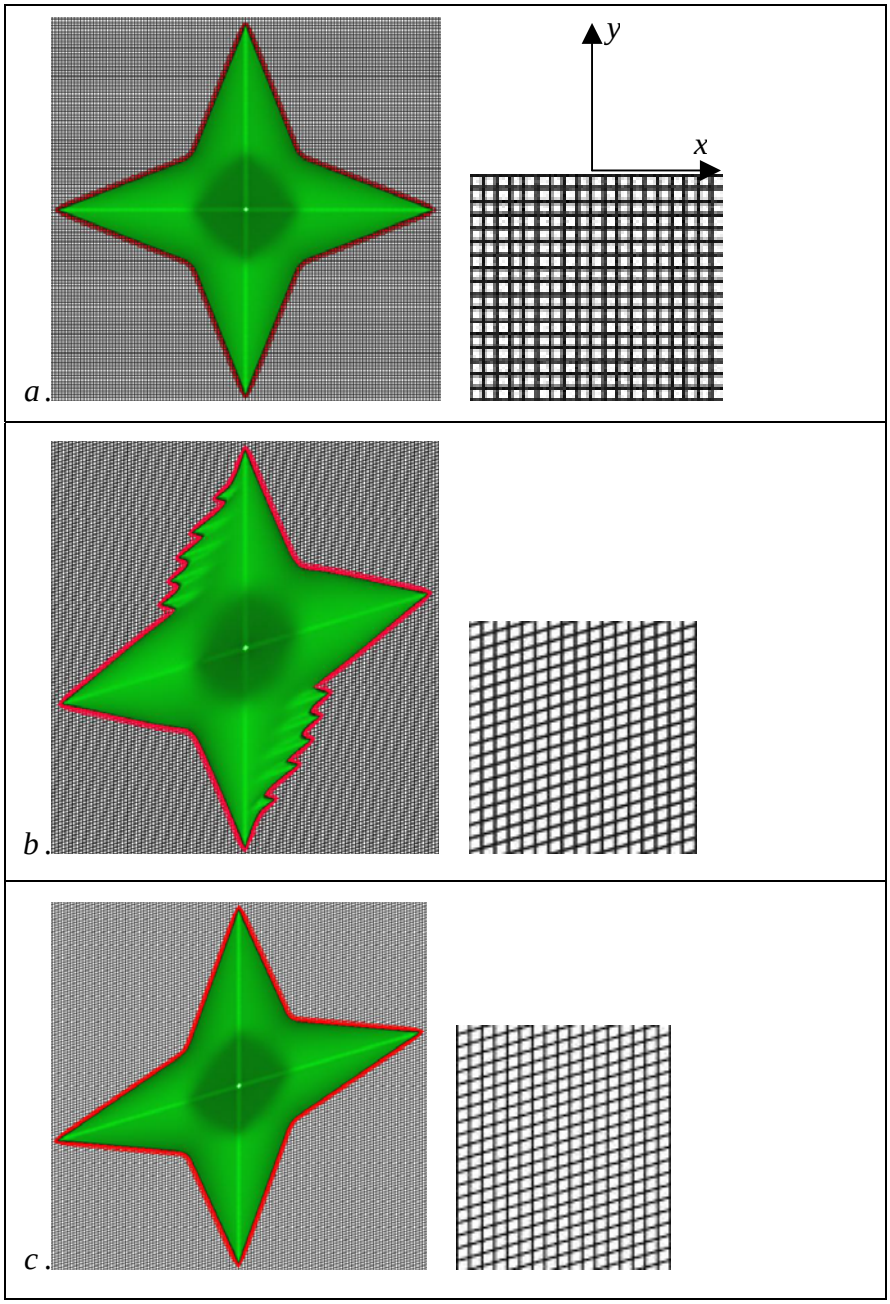

Figure 3.10: Cross-section in z-direction of grain: (a) no deformation; (b) Simple shear deformation while grain growth; (c) simple shear deformation after grain growth

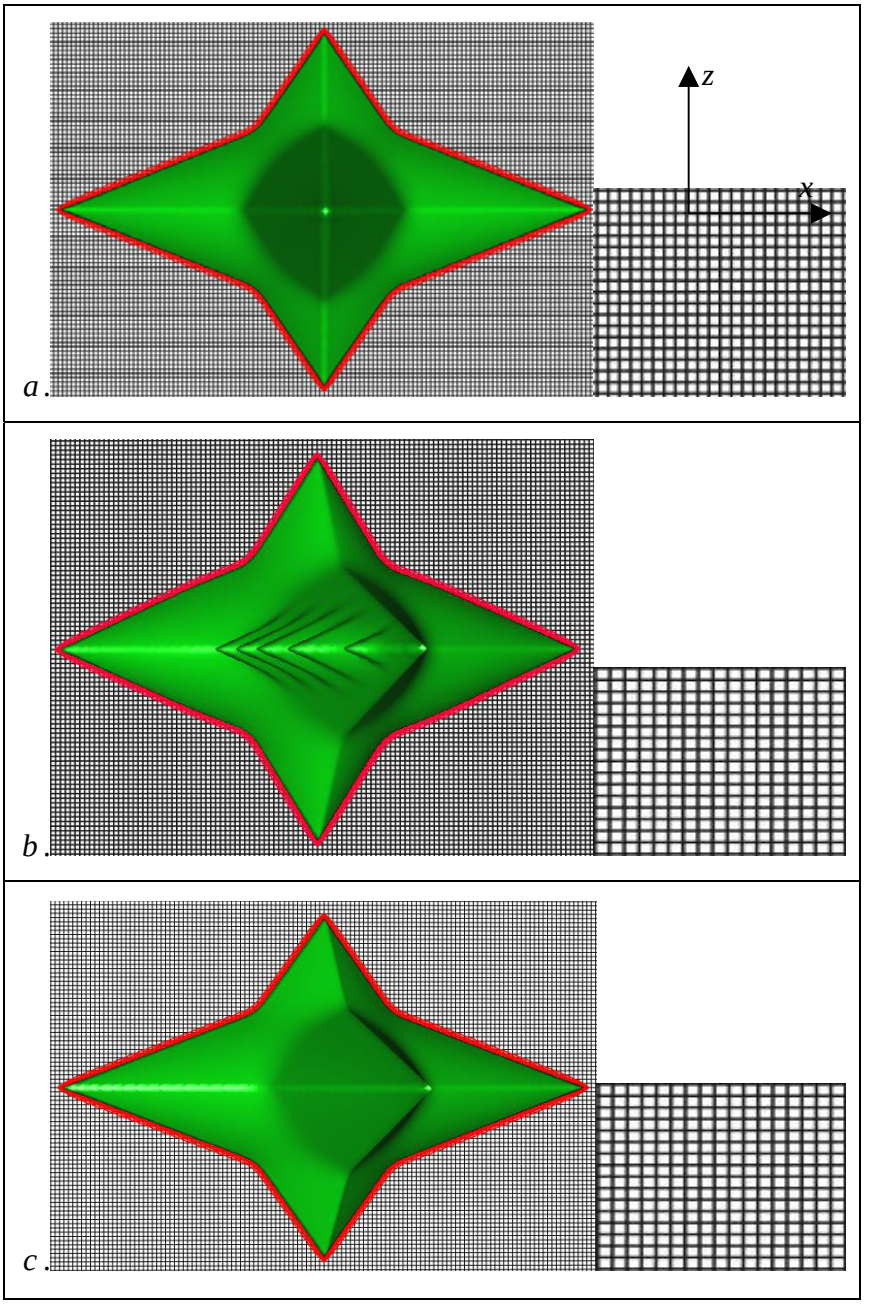

Figure 3.11: Cross-section in y-direction of grain: (a) simple shear deformation while grain growth; (b) simple shear deformation after grain growth.

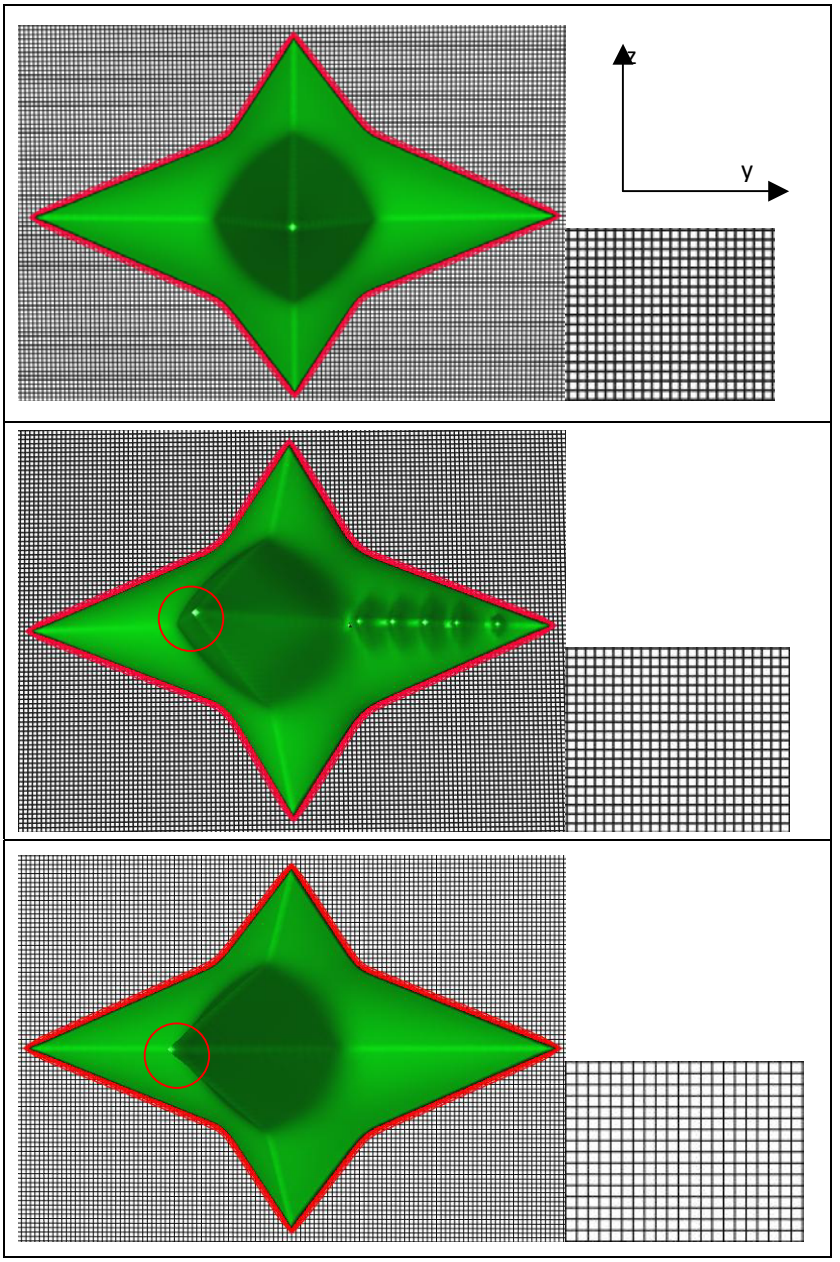

Figure 3.12: Cross-section in x-direction of grain: (a) No deformation; (b) Simple shear deformation while grain growth; (c) Simple shear deformation after grain growth.

In simple shear deformation, the shearing force is applied to a body the amount of slide or shear between two layers unit distance apart is shear strain. Hook's law states that stress is proportional to strain within the elastic limit, that is, within the range of forces where the body will recover its original shape when the forces are removed. Furthermore, if a material is strained in a particular direction the crystallites will usually be elongated in the same direction. In Figure 3.9, the simple shear deformation is in $\hat{y}$ axis which changes the position of each points in $\hat{y}$ direction. From the lattice sections of each direction in Figure 3.10, 3.11 and 3.12, lattices distorted in xy plane and elongated in xz plane.

In xy plane, meshed are distorted because of the simple shear deformation along $\hat{y}$ axis. The normal vector of the interface is changed which result the grain growth to different direction. From Figure 3.13, after simple shear deformation, grain growth according to the new vector $\hat{n}'$ which result the new microstructure.

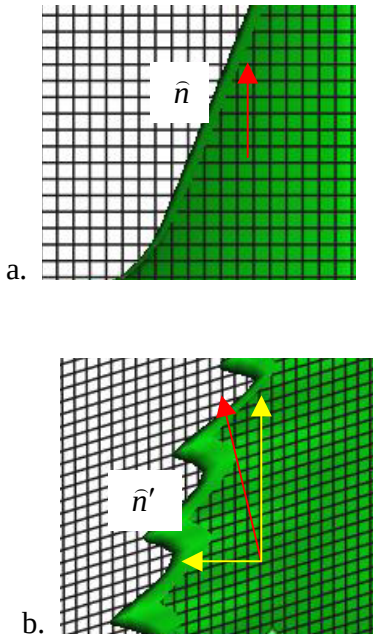

Figure 3.13: Normal vector of interface. (a) No deformation. (b) During deformation. $\hat{n}$ means normal vector of the interface before deformation. $\hat{n}'$ represents the new normal vector after deformation.

In xz plane, there is no as big difference of microstructure as in yz plane. The distances of the lattice elongate in $\hat{x}$ direction and shorten in $\hat{z}$ direction. This results diffusion of phase-field parameter ϕ in $\hat{z}$ direction a little bit faster than it in deformation after grain growth. Therefore, the grain growth is faster in $\hat{z}$ direction which also showed in Figure 3.12.

In *yz* plane, there is no lattice change which result the same microstructure evolution.

In conclusion, the strain will usually tend to partially orient the distorted crystallites. The glide planes and glide directions in crystallites tend to become parallel to the deformation direction. In material, such preferential orientation is called texture. Texture will often persist through subsequent recrystallization. In this simulation, after once deformation, the grain growth direction changes and persists in new direction before second deformation.

In cubic and isotropic situation, there are no big differences in microstructure evolution because their anisotropy of interface energy is small.

Actually, in most of the solid materials, the individual crystals are rather small and materials contain many of these crystallites. Each of these crystallites is misoriented with respect to its neighbours to a greater or lesser degree. Often these crystallites are called grains, and the regions between crystallites are called grain boundary, where nucleation has more chances to happen than inside the grains. Figure 3.14 illustrates how nucleation happens in the grain boundary [20]. From the simulation results, deformation happens during phase transition makes different area of grain boundary and this changes

the density of sites for nucleation.

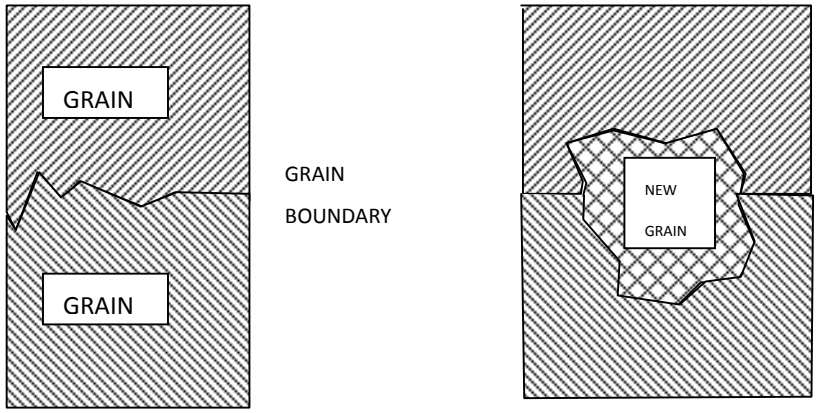

Figure 3.14. Schematic of nucleation at grain boundary

Solid-solid growth during deformation process, a desired orientation can be obtained by controlling the deformation value and direction so that the single crystal region can bear the desired spatial relation to the axes of the specimen. Therefore, a new microstructure can be obtained to make new physical properties.

3.4 Conclusion

The physical properties of all technologically interesting materials are strongly dependent upon their chemical composition as well as their microstructure. The most efficient way of obtaining the desirable microstructure is via accurate control of phase transformation in solids. Phase transition requires two processes: nucleation and growth. Nucleation involves the formation of very small particles. During growth, the nuclei grow in size at the expense of the surrounding material.

The structure resulting from a solid state phase transformation depends on the crystallographic relationship between the lattices of the initial and product phases, on the physical properties of the separate phases, and on the rate of the transformation. There are many phase transformations which are not limited by diffusion, but result simply from some form of mechanical instability of the crystal lattices, and may require some form of structural transition from one crystallographic lattice to another. Thus, a homogeneous movement of many atoms may results in a change in crystalline structure by introducing an entirely new lattices and corresponding unit cell. During the movements the atoms typically maintain their relative relationships which are showed in the results.

According the results of the simulation, a new microstructure is obtained which can give us new physical properties. There is no mass diffusion in this model. Thus, in the further work, basic on this model we can add composition diffusion and simulation more crystal in one system which related to the texture.

Chapter 4

Conclusion

The effect of various deformations in phase transition is important because it can change the way of grain growth. The aim of this work was to simulate the effect of homogeneous deformation in phase transition. First we described the problem of calculating the microstructure evolution for homogeneous deformation and then provided a detailed numerical method and methodology for solving the three-dimension phase-field model to simulate such microstructure evolution in phase transition while warm rolling.

From this work, we know homogeneous deformation in phase transition will cause not only the change of lattice geometry used in phase-field model but also cause the grain distortion which related with the interface migration pattern. Subsequently, the microstructure that obtained by phase transition during warm rolling can be completely different from that rolling after phase transition.

Metal with new microstructure and therefore new properties can be obtained by this processing.

Meanwhile, in the process of simulation, phase-field model combined finite difference method, viewed solely as a framework motivated by the physics of deformation in the microstructure, provides the finite difference analyst benefit as compared to the more common model. The simulation captures the underlying physics of metal deformation to a greater degree.

The whole work provides a method to simulate phase-field model in irregular lattice using general finite difference method. And the results of the simulation show that the microstructure evolution of deformation while phase transition could be different compared with deformation after phase transition.

REFERENCES

1. Haldar and R.K. Ray. Microstructural and textural development I: an extra low carbon steel during warm rolling, *Mater. Sci. Eng. A* 391 (2005), p. 402.

2. G.H. Akbari, C.M. Sellars and J.A. Whiteman. *Acta Mater*. 45 (1997), p. 5047–5058.

3. J Majta and A.K. Zurek. Modeling of ferrite structure after deformation in the two-phase region, *Int. J. Plasticity* 19 (2003), p. 707–730.

4. B.Koohbor, D.Ohadi, S.Serajzadeh and J.M.Akhgar. Effect of rolling speed on the occurrence of strain aging during and after warm rolling of a low-carbon steel. *Journal of Material Science* (2009), p. 3405-3412

5. D. Liu, A.O. Humphreys, M.R. Toroghinezhad and J.J. Jonas. The Deformation Microstructure and Recrystallization Behavior of Warm Rolled Steels; *ISIJ Intl*., 42, (2002), p. 751-759.

6. S. Serajzadeh and M. Mohammadzadeh. Effects of deformation parameters on the final microstructure and mechanical properties in warm rolling of a low-carbon steel, *Int. J. Adv. Manuf. Tech*. (2006), p. 262-269

7. N. Moelans, B. Blanpain, P.Wollants, Calphad, An introduction to phase-field modeling for microstructure evolution. Vol. 32: 268-294 (2008)

8. J. Fix, in Free Boundary Problems: Theory and Applications, Ed. A. Fasano and M. Primicerio, p. 580, Pitman (Boston, 1983)

9. J.S. Langer, Models of pattern formation in first–order phase transitions, in Directions in Condensed Matter Physics p. 165, Ed. *World Scientific, Singapore*, (1986)

10. John W. Cahn and John E. Hilliard. Free energy of a nonuniform system. Nucleation in a two-component incompressible fluid. *The Journal of Chemical Physics*. (1959). p. 688-699

11. Cahn, J.W., On spinodal decomposition in cubic crystals, *Acta Met*., Vol. 10, p. 179 (1962)

12. A. A. Wheeler, W. J. Boettinger and G. B. McFadden. Phase-field model for isothermal phase transition in binary alloys. *Physical Review A*. Vol. 45, p. 7424-7439 (1992)

13. J. A. Warren and W. J. Boettinger. Prediction of dendritic growth and microsegegation patterns in a binary alloy using the phase-field method. *Acta metal*. Vol. 43, p. 689-703 (1994)

14. A.A. Wheeler, B.T. Murray and R.J. Schaefer. Computation of dendrites using a phase field model, *Physica D* (1993), p. 243–262.

15. J. W. Cahn and D. W. Hoffman, "A Vector Thermodynamics for Anisotropic Surfaces. II. Curved and Facetted Surfaces," *Acta Met.* 22, 1205-1214 (1974).

16. R.S. Qin and H.K.D.H. Bhadeshia. Phase-field model study of the effect of interface anisotropy on the crystal morphological evolution of cubic metals. *Acta Mater* 57 (2009), p. 2210.

17. A. A. Wheel, W. J. Boettinger and G. B. McFadden. Phase-field model for isothermal phase transition in binary alloys. *Phys. Rev. A* 45, 7424 (1992).

18. Seong Gyoon Kim, Won Tae Kim and Toshio Suzuki. Interfacial compositions of solid and liquid in a phase-field model with finite

interface thickness for isothermal solidification in binary alloys. *Phys. Rev. E.* 58, 3316-3323. (1998)

19. Chae Jae-Yong, R.S. Qin, H.K.D.H. Bhadeshia. Topology of the Deformation of a Non-uniform Grain Structure. *ISIJ international*. 49(2009), p.115-118

20. R. A. Laudise. The growth of single crystals. (1970)

21. Q. Zhu, C.M. Sellars, and H.K.D.H. Bhadeshia. Quantitative metallography of deformed grains. *Materials Science and Technology,* 23 (2007), p. 757-766

22. R.S. Qin, E.R. Wallach and R.C. Thomson. A phase-field model for the solidification of multicomponent and multiphase alloys. J Cryst Growth 279 (2005), p. 163.

23. J.A. Warren and W.J. Boettinger. Prediction of dendritic growth and microsegregation patterns in a binary alloy using the phase-field method. *Acta Metall Mater* 43 (1995), p. 689.

24. R. S. Qin and H.K.D.H. Bhadeshia. Phase-field model in materials science.

25. Mikhail Shashkov and Stanly Steinberg. Conservative Finite-Difference Methods on General Grids. (1996), p. 26-45.

26. Yang Z, Johnson RA. *Modelling Simul Mater Sci Eng*. (1993). p. 707-716

27. J. Fridbery, L.D. Torndahl and M. Hillert, Diffusion in iron. Jernkont. Ann. 153 (1969), p. 263–276.

28. C.A. Greene and S. Ankem. Modelling of elastic interaction stresses in two-phase materials by FEM, *Mater Sci Eng A* 202 (1995), p. 103–111

29. M.M. Tong, J. Ni, Y.T. Zhang, D.Z. Li and Y.Y. Li. Coupled simulation of the influence of austenite deformation on the subsequent isothermal austenite-ferrite transformation, *Metall Mater Trans A* 35A (2004), p. 1565

30. R.S. Qin and E.R. Wallach. A phase-field model coupled with a thermodynamic database. *Acta Mater*. 51 (2003), p. 6199.

Appendix A

This is the documentation for the program in this work

Program

TX_PHASE-FIELD MODEL_HOMOGENEOUS DEFORMATION

1. Provenance
2. Purpose
3. Sepecification
4. Description
5. References
6. Parameter
7. Error indicatiors
8. Accuracy estimate
9. Further comments
10. Example
11. Auxiliary routines
12. Keywords

1. Provenance of Source code

Tan Xu, Rongshan Qin and H.K.D.H. Bhadeshia

Graduate Institute of Ferrous Technology (GIFT)

Pohang University of Science and Technology

Pohang, Kyngbuk, Republic of Korea

tanx03@postech.ac.kr

2. Purpose

To simulate microstructure evolution in warm rolling by combining phase-field model with homogeneous deformation. Furthermore, compared the results with microstructure in homogeneous deformation after homogeneous deformation.

3. Specification

Language: C++

Product form: Executables and complete source code

4. Description

A method to simulate materials rolling at two-phase region has been developed. The characteristics of this processing is that the

phase transition and hence the crystal growth is taking place when system undergoing deformation. The microstructure evolution is handled by phase-field model. Various deformations are accommodated by grid transformations. The methodology and mathematics for achieving this simulation are presented in details. Numerical study demonstrates convincing results. It is found that the deformation-induced interface disruption plays the dominant role in growth of crystals with strong interface anisotropy.

The program runs best on Microsoft Visual C++ compiler

All the files are compressed into a file called

Microstructure_warm rolling. tar

The .tar file contains the following files

TX_CalcBasicFunctions.h **TX_CalcIO.H** **TX_CalcParameters.h** **TX_CalcPhaseField.h** **TX_Deformation.h**	Header files for variables
TX_CalcMain.cpp	Main module.
TX_CalcPhaseField.cpp **TX_Deformation.cpp**	Calculation about the phase-field parameters. Degree of the the type of deformation, and other values needed are selected here
TX_parameters.dat	File of the input parameter
Simq.dat **Simgrid.dat**	Output files which contain the calculation results and shape of unit cell. File names are determined by the grain generating degree.
TX_PD.exe	Executive file

5. Reference

Zhu, Q., Sellars, C. M. and Bhadeshia, H. K. D. H. : Quantitative metallography of deformed grains, *Material Science and Technology*, Vol. 23 (2007) pp. 757-766

R.S. Qin and H.K.D.H. Bhadeshia. Phase-field model study of the effect of interface anisotropy on the crystal morphological evolution of cubic metals. *Acta Mater* 57 (2009), p. 2210.

Jae-Yong, C., Rongshan, Q. and Bhadeshia, H. K. D. H. : Topology of the deformation of a non-uniform grain structure, submitted to *Material Science and Technology.*

R.S. Qin and E.R. Wallach. A phase-field model coupled with a thermodynamic database. Acta Mater. 51 (2003), p. 6199.

6. Parameters

Input parameters:

The input variables are determine before compile

total_grid_x/y/z : size of unit cell

save_time_steps: time for output files

time_to_deformation: deformation time

deform_Case: deformation mode

deformation_value: determine the deformation matrix

Output parameters

Vertex coordinate are listed in **simgrid.dat**. array of three numbers which represent x, y and z respectively are repeated.

The calculation results about phase-field parameter ϕ are printed in **simq.dat** files.

7. Error indicators

None

8. Accuracy

No information

9. Further comments

Composition diffusion will be added into the model

10. Example

a. Set value of unit cell size, *deform_case deformation_value and time_to_deformation*

total_grid_x	**160**
total_grid_y	**160**
total_grid_z	**120**
total_phase	2
total_solute	0
total_time_steps	500001
save_time_span	2000
time_to_deformation	**6000**
deform_Case	**4**
deformation_value	**0.5**
grid_distance	7.15E-9
half_interface_thick	1.43E-8
molar_volume	7.18E-6
interface_energy_0	0.8
phase_mobility_0	100.0
bulk_free_energy_0	-1.730326E+9
bulk_free_energy_1	-2.088922E+9

b. Compile

c. Run "**TX_PD.exe**"

d. "**simgrid.dat**" and **"smq.dat**" are generated.

Simgrid.dat
60 60 60 0 0.715 1.43 2.145 2.86 3.575 4.29 5.005 5.72 6.435 7.15 7.865 8.58 9.295 10.01 10.725 11.44 12.155 12.87 13.585 14.3 15.015 15.73 16.445 17.16 17.875 18.59 19.305 20.02 20.735 21.45 22.165 22.88 23.595 24.31 25.025 25.74 26.455 27.17 27.885 28.6 29.315 30.03 30.745 31.46 32.175 32.89 33.605 34.32 35.035 35.75 36.465 37.18 37.895 38.61 39.325 40.04 40.755 41.47 42.185 0 0.715 1.43 2.145 2.86 3.575 4.29 5.005 5.72 6.435 7.15 7.865 8.58 9.295 10.01 10.725 11.44 12.155…

Simq.dat
…0 0 0

11. Auxiliary rountines

None

12. Keywords

Phase-field parameter, homogeneous deformation

Acknowledgements

I would like to express my deep thanks to Professor Rongshan, Qin and Professor H.K.D.H. Bhadeshia for their supervision, encouragement and help. And thanks to Professor Barlat, Frederic, Professor In Gee Kim and Professor Suh, Dong-Woo for their great support, advice and friendship.

Thanks all the members in Computational Metallurgy Laboratory for helping me so much. Their kindly help and great friendship will always on my mind.

I am also appreciating Graduate Institute of Ferrous Technology and POSCO for their financial support.

Finally, thanks to my parents for everlasting support for me.

CURRICULUM VITAE

Name: Tan Xu (谭旭)

Date of birth: 9th, July 1984

Place of birth: GuiZhou Province, P.R. CHINA

Education:

M.S. POSTECH (Pohang, Korea), Graduate Institute of Ferrous Technology, Computational Metallurgy.

B.S. 2007 Tsinghua University (Beijing, P. R. China), Engineering Physics.